NASA Contractor Report 3962

An Exact Solution for the Solidification of a Liquid Slab of Binary Mixture

B. N. Antar, F. G. Collins,
and A. E. Aumalis
The University of Tennessee Space Institute
Tullahoma, Tennessee

Prepared for
George C. Marshall Space Flight Center
under Contract NAS8-34268

National Aeronautics
and Space Administration

**Scientific and Technical
Information Branch**

1986

FOREWORD

The work reported here concerning formulation and solution of a two phase mixed Stephan problem is relevant to alloy solidification and crystal growth processes such as those being investigated in low gravity experiments aboard orbiting laboratories. The work was supported by the Atmospheric Science Division of the Systems Dynamics Laboratory at the Marshall Space Flight Center.

TABLE OF CONTENTS

LIST OF FIGURES

LIST OF SYMBOLS

d_0	depth of slab
d	solute diffusivity
C	concentration
C_p	specific heat
h	heat transfer coefficient
k	thermal conductivity
$\hat{k}$	partition coefficient
ℓ	latent heat
m	slope of solidus-liquidus line in phase diagram
S	interface
T	temperature
t	time
z	distance
κ	thermal diffusivity
ρ	density

CHAPTER I

INTRODUCTION

Heat transfer problems dealing with the melting or freezing of a substance have received a lot of attention for more than a century. The problem is characterized by a moving surface of separation between the two phases, with release or absorption of latent heat at this interface. Of interest are the position of this interface with respect to time and the temperature distributions in both phases. This class of problems are generally referred to as the Stefan problem.

The simplest problem in this area is the one-dimensional solidification in a semi-infinite region. The first published work is by G. Lame and B. P. Clapeyron (1831) [17],[1] which dealt with determining the thickness of the solid crust generated by the cooling of a liquid initially at constant temperature. They found the position of the interface to move proportionally to the square root of time, but they did not find the constant of proportionality. The first known solutions for this problem were found by Neumann (1860) and Stefan (1889) [6]. The solution takes the form of error integrals and the position of the interface was found to be $S(t) = 2\lambda\sqrt{\kappa_s t}$, where κ_s is the thermal diffusivity, and λ is determined by the conservation of energy equation at the interface.

Further complications arise when the material freezing is an alloy. The classical Stefan problem normally has three unknowns,

---

[1]Numbers in brackets refer to similarly numbered references in the List of References.

namely, the interface position and the temperatures of both phases. The melting temperature of an alloy is strongly dependant on the composition at the interface. Therefore, freezing (or melting) can occur over a range of temperature. That, and the concentration distributions of the two phases, adds three more unknowns to the problem. Work done by Tao [18] considers this problem with an arbitrarily prescribed heat flux at the lower boundary. His closed form solution is comprised of an infinite sum of error functions.

When considering a slab of finite depth, the similarity transformation, in general, cannot be applied and no known closed form solution exists. Boley [3] has formulated a solution for the system as it first undergoes solidification. However, once the effects of freezing have reached the upper surface the solution is no longer valid. To describe the system for all time, we must resort to numerical approximation techniques. Meyer [11,12] has developed an algorithm using the Implicit Imbedding technique that solves the problem of the slab, but does not take into consideration the case of alloy solidification.

The study presented here considers alloy solidification in a finite slab, with heat dissipation from both the upper and lower surfaces by convection. Though the governing equations are linear, these interfacial conditions are not, making this a non-linear problem. Another complication will be added, that of allowing for density differences between solid and liquid phases. This causes a moving upper boundary as well as the moving interface. We see this solution as an extension of Meyer's method. Two methods of solutions will be

presented. One, a purely numerical technique, makes use of a Runge-Kutta integrator to solve the equations generated by Meyer's method. This solution failed at the low diffusion rates of solids because of the stiffness of the equations. The second solution is an analytical method. Closed form solutions were found of the basic equations, though quadrature techniques were still required. This enabled us to reach lower diffusion rates, though not as low as desired, because of accuracy limitations of the quadrature technique.

Stefan type problems have significant importance to many industrial processes. In the production of steel billets [14], carbon within the metal oxidizes at the surface setting up strong concentration gradients that cause more carbon to diffuse to the surface. This outer layer is no longer of the same type steel and would have to be ground off. Determining and minimizing the depth of this layer is necessary for the reduction of costs. Corrosion problems are similar in behavior. In the manufacture of glass [14], heat transfer rates must be optimized to limit crystal growth and reduce the formation of gas bubbles. Recently, much interest has been generated in the possibility of processing materials in space. In the reduced gravity environment, it would be possible to produce large crystals of uniform properties and to manufacture materials with unique properties.

CHAPTER II

PROBLEM FORMULATION

In this chapter we will discuss the formulation of the basic equations for the two phase mixed Stefan problem. Exact solutions by Neumann and Stefan and the numerical technique by Meyer will be reviewed. For the mixed Stefan problem we will consider a slab consisting of a binary liquid alloy, initially at constant temperature, T_0. The slab is of finite depth, d_0, and infinite width (Figure 1). Heat is to be removed from both the upper and lower surfaces, with solidification starting at the lower surface. The problem is characterized by a moving interface, S(t), between the solid and liquid phases, with latent heat release at the interface. The equations will allow for different densities for the solid and liquid causing a volume change and therefore a moving upper surface during freezing. The upper and lower surfaces will be closed to any mass flow and mass diffusion in the solid and liquid will be investigated. Since the substance is an alloy, the freezing temperature will be dependant on the composition at the interface. A sketch of this model is shown in Figure 1.

The governing equations for the temperature and concentration distributions when there is a change in volume during solidification ($\rho_s/\rho_\ell \neq 1$) take the form [6]:

$$\frac{\partial T_\ell}{\partial t} - \left(\frac{\rho_s}{\rho_\ell} - 1\right) \frac{dS}{dt} \frac{\partial T_\ell}{\partial z} = \kappa_\ell \frac{\partial^2 T_\ell}{\partial z^2} \tag{1}$$

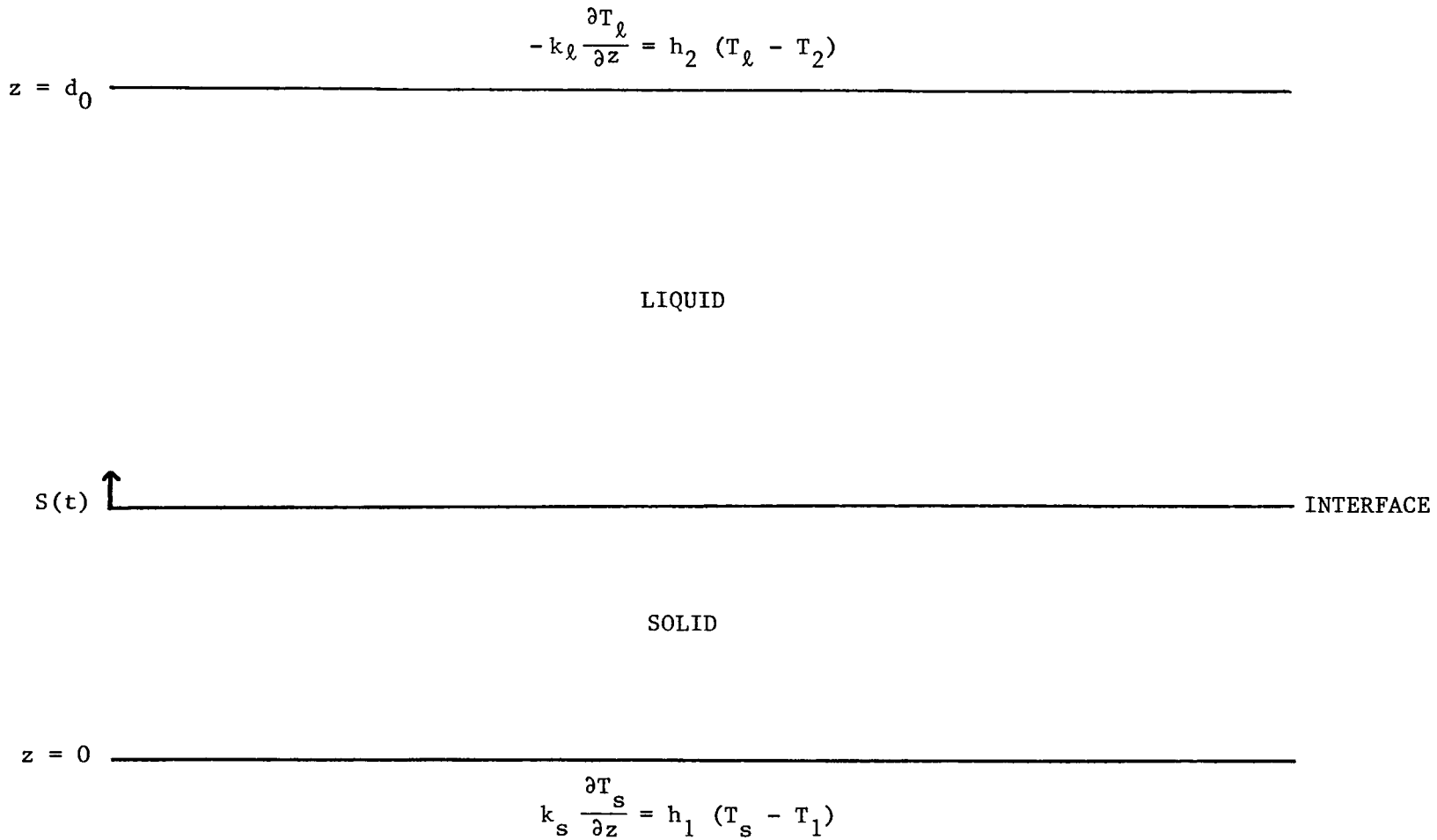

Figure 1. Sketch of theoretical model.

$$\frac{\partial C_\ell}{\partial t} - \left(\frac{\rho_s}{\rho_\ell} - 1\right) \frac{dS}{dt} \frac{\partial C_\ell}{\partial z} = d_\ell \frac{\partial^2 C_\ell}{\partial z^2} \tag{2}$$

in the liquid, and

$$\frac{\partial T_s}{\partial t} = \kappa_s \frac{\partial^2 T_s}{\partial z^2} \tag{3}$$

$$\frac{\partial C_s}{\partial t} = d_s \frac{\partial^2 C_s}{\partial z^2} \tag{4}$$

in the solid. C denotes the solute concentration and T the temperature. S(t) is the interface position and ρ, κ and d denote the density, thermal diffusivity and solute diffusivity. The subscripts s and ℓ denote solid and liquid, respectively.

The interface conditions are:

$$k_s \frac{\partial T_s}{\partial z} - k_\ell \frac{\partial T_\ell}{\partial z} = \rho_s \ell \frac{dS}{dt} \tag{5}$$

$$\rho_s d_s \frac{\partial C_s}{\partial z} - \rho_\ell d_\ell \frac{\partial C_\ell}{\partial z} = \rho_s C_\ell (1 - \hat{k}) \frac{dS}{dt} \tag{6}$$

Equations (5) and (6) are the conservation of energy and mass equations at the interface. k, $\hat{k}$ and ℓ are the thermal conductivity, the partition coefficient and the latent heat. Also at the interface, both the solid and liquid must be at the equilibrium melting temperature, T_m, and the proper value of solute concentration which may be described by

$$T_m = T_i - mC_\ell \tag{7}$$

$$C_s = \hat{k}C_\ell \tag{8}$$

Equation (7) implies that the melting temperature of the alloy is a linear function of concentration. Looking at the phase diagram, Figure 2 [1], we can see that this is a simplification of the actual relationship. The decrease in the melting temperature with increase in concentration can be rather closely approximated by a linear function. However, at a certain concentration the melting temperature will begin to increase. Since the method of solution does not depend on this equation, a more complicated expression could be substituted, but will not be for this work.

The boundary conditions at the upper and lower surfaces take the form:

at $z = 0$

$$k_s \frac{\partial T}{\partial z} = h_1 (T_s - T_1) \tag{9}$$

$$\frac{\partial C}{\partial z} = 0 \tag{10}$$

at $z = d_0 - (\frac{\rho_s}{\rho_\ell} - 1)\, S(t)$

$$-k_\ell \frac{\partial T}{\partial z} = h_2 (T_\ell - T_2) \tag{11}$$

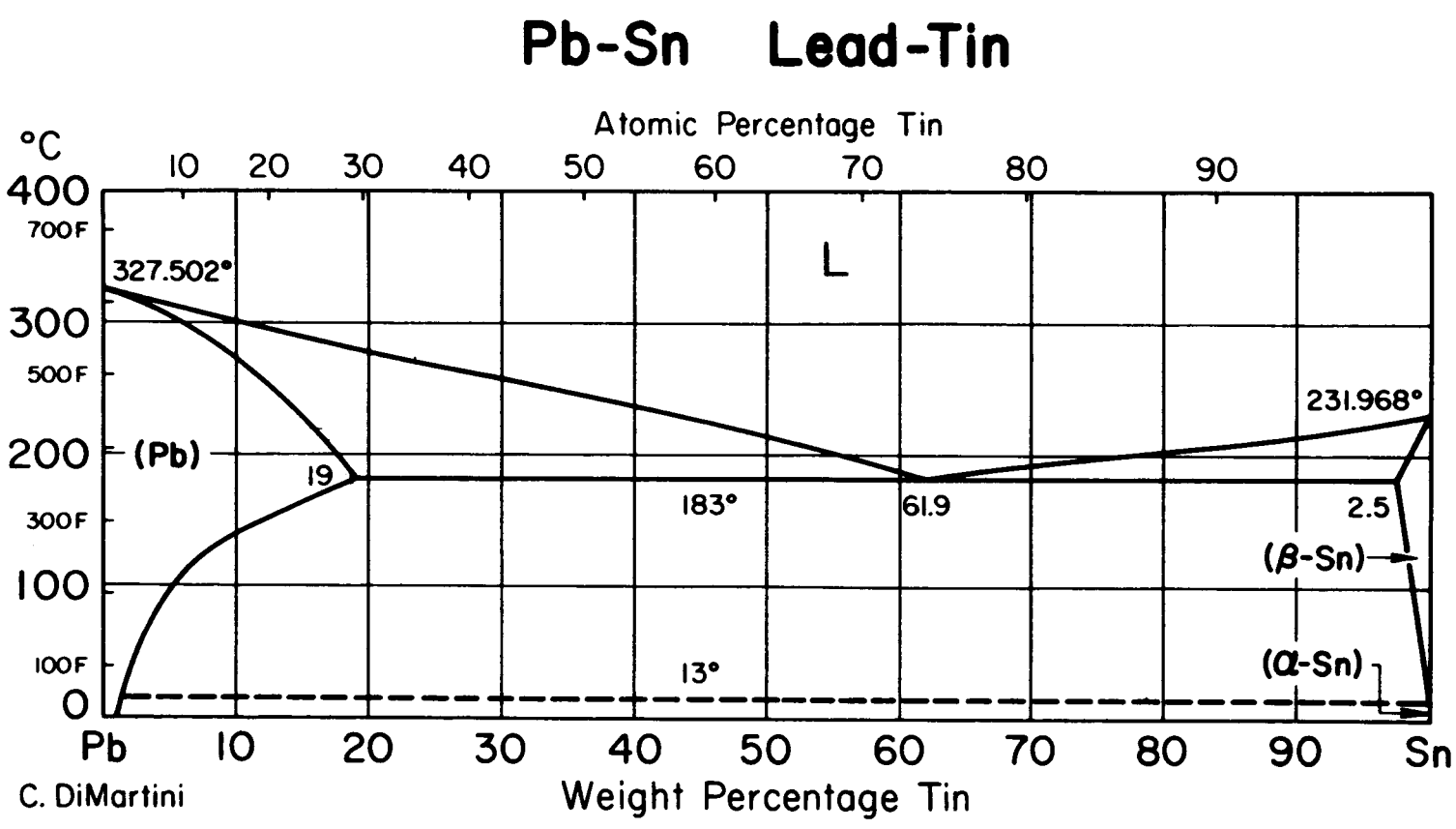

Figure 2. Pb-Sn Phase diagram.

$$\frac{\partial C}{\partial z} = 0 \tag{12}$$

where subscripts 1 and 2 denote lower and upper surfaces, respectively. Equations (9) and (11) represent heat dissipation from the surfaces by convection into a medium at temperatures T_1 and T_2, respectively.

The Solutions of Neumann and Stefan

The first solutions for the Stefan problem, in a semi-infinite space, were found by Neumann in 1860 and Stefan in 1889 [6]. The governing equations are (1), (2), and interface condition (5). They do not allow for a density change between the solid and liquid, i.e., $\rho_s = \rho_\ell$. The boundary conditions at zero and ∞ are

$$T_\ell = T \text{ at } z \to \infty$$

$$T_s = 0 \text{ at } z = 0$$

The solutions

$$T_\ell = T - B\,\mathrm{erfc}\left(\frac{z}{2\sqrt{\kappa_s t}}\right)$$

$$T_s = A\,\mathrm{erf}\left(\frac{z}{2\sqrt{\kappa_s t}}\right)$$

satisfy the basic equations and boundary conditions at zero and ∞, where A and B are constants of integration. Using the interface condition

$$T_s = T_\ell = T_m \text{ at } z = s$$

we have

$$\text{Aerf}\left(\frac{s}{2\sqrt{\kappa_s t}}\right) = T - \text{Berfc}\left(\frac{s}{2\sqrt{\kappa_s t}}\right) = T_m$$

For this to be valid for all t, we must have

$$\frac{s}{2\sqrt{\kappa_s t}} = \lambda = \text{constant}$$

or

$$s = 2\lambda\sqrt{\kappa_s t}$$

rewriting the solution at the interface, we have

$$\text{Aerf}(\lambda) = T - \text{Berfc}\left(\lambda\sqrt{\frac{\kappa_s}{\kappa_\ell}}\right) = T_m$$

which determines the constants A and B as follows:

$$A = \frac{T_m}{\text{erf}(\lambda)}$$

$$B = \frac{T - T_m}{\text{erfc}\left(\lambda\sqrt{\frac{\kappa_s}{\kappa_\ell}}\right)}$$

Now, using the interface condition (5), we can evaluate the constant λ:

$$\frac{\exp(-\lambda^2)}{\operatorname{erf}(\lambda)} - \frac{k_\ell}{k_s}\sqrt{\frac{\kappa_s}{\kappa_\ell}}\,\frac{T - T_m}{T_m}\,\frac{\exp\left(-\frac{\kappa_s\lambda^2}{\kappa_\ell}\right)}{\operatorname{erfc}\left(\lambda\sqrt{\frac{\kappa_s}{\kappa_\ell}}\right)} = \frac{\lambda\ell\sqrt{\pi}}{C_{p_s}T_m}$$

Stefan's solution assumes the liquid is initially at the melting temperature ($T = T_m$), giving the equation for λ as

$$\lambda\exp(\lambda^2)\operatorname{erf}(\lambda) = \frac{C_{\rho_s}T_m}{\ell\sqrt{\pi}}$$

Adding the change in density term ($\rho_s/\rho_\ell - 1$), so that the basic equation matches equation (1), changes the solution in the liquid region to the following:

$$T_s = T - B\operatorname{erfc}\left[\frac{z}{2\sqrt{\kappa_\ell t}} + \lambda\left(\frac{\rho_s}{\rho_\ell} - 1\right)\sqrt{\frac{\kappa_s}{\kappa_\ell}}\right]$$

with

$$B = \frac{T - T_m}{\operatorname{erfc}\left(\lambda\frac{\rho_s}{\rho_\ell}\sqrt{\frac{\kappa_s}{\kappa_\ell}}\right)}$$

and the equation to determine λ:

$$\frac{\exp(-\lambda^2)}{\operatorname{erf}(\lambda)} - \frac{(T - T_m)k_\ell \exp\left(-\frac{\lambda^2 \rho_s^2 \kappa_s}{\rho_\ell \kappa_\ell}\right)}{T_m k_s \operatorname{erfc}\left(\lambda \sqrt{\frac{\kappa_s}{\kappa_\ell}} \frac{\rho_s}{\rho_\ell}\right)} \sqrt{\frac{\kappa_s}{\kappa_\ell}} = \frac{\lambda \ell \sqrt{\pi}}{C_{p_s} T_m}$$

Numerical Technique, the Method of Meyer

When considering a slab of finite depth, a numerical technique must be employed. In a series of papers Meyer [11,12] has developed one such technique using the Invariant Imbedding Method. This technique also allows for the use of non-linear boundary conditions. The governing equations are (1) and (3), with interface conditions (5), and boundary conditions (9) and (11). Since numerical methods are used, it is convenient to first nondimensionalize the equations. The following substitutions were made:

$$R = \frac{\rho_s}{\rho_\ell} \qquad D = \frac{d_s}{d_\ell}$$

$$C = \frac{C}{C_0} \qquad P_\ell = \frac{d_\ell}{\kappa_\ell} = \text{Lewis Number}$$

$$M = \frac{C_0}{T_1 - T_0}\, m \qquad P_s = \frac{d_s}{\kappa_s} = \text{Lewis Number}$$

$$K = \frac{\kappa_s}{\kappa_\ell} \qquad B_i = \frac{h_i d_0}{k_\ell} = \text{Biot Modulus}$$

$$z = \frac{z}{d_0} \qquad L = \frac{\ell}{C_{p_\ell}(T_1 - T_0)}$$

$$\Lambda = \frac{k_s}{k_\ell} \qquad \Psi = \frac{T_2 - T_0}{T_1 - T_0}$$

$$\Theta = \frac{T - T_0}{T_1 - T_0} \qquad \tau = \frac{\kappa_\ell}{d_0^2} t$$

After nondimensionalization, the governing equations, interface and boundary conditions take the form

$$\frac{\partial \Theta_\ell}{\partial \tau} - (R - 1) \frac{dS}{d\tau} \frac{\partial \Theta_\ell}{\partial z} = \frac{\partial^2 \Theta_\ell}{\partial z^2} \tag{13}$$

$$\frac{\partial \Theta_s}{\partial \tau} = K \frac{\partial^2 \Theta_s}{\partial z^2} \tag{14}$$

$$\Lambda \frac{\partial \Theta_s}{\partial z} - \frac{\partial \Theta_\ell}{\partial z} = RL \frac{dS}{d\tau} \tag{15}$$

$$\frac{\partial \Theta_s(0)}{\partial z} = \frac{B_1}{\Lambda} (\Theta_s - 1) \tag{16}$$

$$\frac{\partial \Theta_\ell(Z_f)}{\partial z} = - B_2(\Theta_\ell + \Psi) \tag{17}$$

Meyer's method consists of first discretizing the time operator in the following manner:

$$\frac{\partial F}{\partial \tau} = \frac{F^N - F^{N-1}}{\Delta \tau}$$

yielding a set of ordinary differential equations, solvable at discrete time steps, N. Next, equations (13) and (14) are rewritten as a first order system.

$$U_\ell = \Theta'_\ell$$

$$\frac{\Theta_\ell^N - \Theta_\ell^{N-1}}{\Delta \tau} - \frac{(R-1)\,(S^N - S^{N-1})}{\Delta \tau} U_\ell = U'_\ell \tag{18}$$

$$U_s = \Theta'_s$$

$$\frac{\Theta_s^N - \Theta_s^{N-1}}{\Delta \tau} = KU'_s \tag{19}$$

where prime denotes differentiation with respect to z. With the conservation of energy equation at the interface taking the form

$$\Lambda \frac{\partial \Theta_s}{\partial z} - \frac{\partial \Theta_\ell}{\partial z} = RL \frac{S^N - S^{N-1}}{\Delta \tau} \tag{20}$$

Now, the Invariant Imbedding technique is used to solve for U_ℓ and U_s. The solution of U_ℓ is assumed to take the form

$$U_\ell^N = Y_\ell^N \Theta_\ell^N + Z_\ell^N$$

then

$$U_\ell^{N'} = Y_\ell^{N'} + Y_\ell^N \Theta_\ell^{N'} + Z_\ell^{N'}$$

$$U_\ell^{N'} = Y_\ell^{N'} + Y_\ell^N \; U_\ell^N + Z_\ell^{N'}$$

These equations are substituted into (18) to yield

$$Y_\ell^{N'} \Theta_\ell^N + (Y_\ell^N)^2 \; \Theta_\ell^N + Y_\ell^N Z_\ell^N + Z_\ell^{N'} = \frac{\Theta_\ell^N}{\Delta\tau} - \frac{\Theta_\ell^{N-1}}{\Delta\tau} - F_R Y_\ell^N \Theta_\ell^N - F_R Z_\ell^N$$

where

$$F_R = \frac{(R - 1) \; (S^N - S^{N-1})}{\Delta\tau}$$

rearranging,

$$Y_\ell^{'} \Theta_\ell^N + (Y_\ell^N)^2 \; \Theta_\ell^N + F_R Y_\ell^N \Theta_\ell^N = - Z_\ell^{N'} - Y_\ell^N \; Z_\ell^N - F_R Z_\ell^N - \frac{\Theta_\ell^{N-1}}{\Delta\tau}$$

from this we get the equations for Y_ℓ and Z_ℓ.

$$Y_\ell^{N'} = - (Y_\ell^N)^2 - F_R Y_\ell^N + \frac{1}{\Delta\tau} \tag{21}$$

$$Z_\ell^{N'} = - Y_\ell^N \; Z_\ell^N - F_R Z_\ell^N - \frac{\Theta_\ell^{N-1}}{\Delta\tau} \tag{22}$$

The boundary conditions are derived similarly.

$$U_\ell^N = Y_\ell^N \; \Theta_\ell^N + Z_\ell^N$$

is substituted into (17) to yield

$$Y_{\ell}^{N}\ (Z_f)\ \Theta_{\ell}^{N}\ (Z_f) + Z_{\ell}^{N}\ (Z_f) = -\ B_2\ (\Theta_{\ell}^{N}\ (Z_f) + \Psi)$$

and therefore

$$Y_{\ell}^{N}\ (Z_f) = -\ B_2$$

$$Z_{\ell}^{N}\ (Z_f) = -\ B_2\Psi$$

where $Z_f = 1 - (R - 1)S^N$. Similarly,

$$U_s^N = Y_s^N\ \Theta_s^N + Z_s^N$$

yields the following equations and boundary conditions:

$$\frac{dY_s^N}{dz} = \frac{1}{K\Delta\tau} - (Y_s^N)^2 \tag{23}$$

$$\text{at } z = 0\ Y_s^N = \frac{B_1}{\Lambda}$$

$$\frac{dZ_s^N}{dz} = -\ Y_s^N\ Z_s^N - \frac{\Theta_s^{N-1}}{K\Delta\tau} \tag{24}$$

$$\text{at } z = 0\ Z_s^N = -\ \frac{B_1}{\Lambda}$$

After solving equations (21)-(24), the temperature distributions can be obtained by solving the following equations:

$$\frac{d\Theta_{\ell}^{N}}{dz} = Y_{\ell}^{N}\ \Theta_{\ell}^{N} + Z_{\ell}^{N} \tag{25}$$

$$\frac{d\Theta_{s}^{N}}{dz} = Y_{s}^{N}\ \Theta_{s}^{N} + Z_{s}^{N} \tag{26}$$

Meyer's Method for the Mixed Problem

Meyer's method can easily be applied to alloy solidification. Equations (2) and (4), interface conditions (6), (7) and (8), and boundary conditions (10) and (12) are nondimensionalized, time operator discretized, and then written as a first order system yielding:

$$V_{\ell} = C'_{\ell}$$

$$\frac{C_{\ell}^{N} - C_{\ell}^{N-1}}{\Delta\tau} - \frac{(R - 1)\ (S^{N} - S^{N-1})}{\Delta\tau} V_{\ell} = P_{\ell} V_{\ell}' \tag{27}$$

$$V_{s} = C'_{s}$$

$$\frac{C_{s}^{N} - C_{s}^{N-1}}{\Delta\tau} = KP_{s} V'_{s} \tag{28}$$

$$RD\ \frac{dC_{s}}{dz} - \frac{dC_{\ell}}{dz} = \frac{R}{P_{\ell}}\ (1 - \hat{k})\ \frac{S^{N} - S^{N-1}}{\Delta\tau} \tag{29}$$

$$\Theta_{m} = \Theta_{i} - MC_{\ell} \tag{30}$$

$$C_{s} = \hat{k} C_{\ell} \tag{31}$$

$$\frac{\partial C_s^N}{\partial z} = 0 \tag{32}$$

$$\frac{\partial C_\ell^N}{\partial z} = 0 \tag{33}$$

V_ℓ and V_s are assumed to have solutions of the form

$$V_\ell^N = X_\ell^N \; C_\ell^N + R_\ell^N$$

$$V_s^N = X_s^N \; C_s^N + R_s^N$$

Then the equations to solve for X_ℓ^N, X_s^N, R_ℓ^N and R_s^N are

$$\frac{dX_\ell^N}{dz} = \frac{1}{P_\ell \Delta\tau} - \frac{F_R}{P_\ell} X_\ell^N - (X_\ell^N)^2 \tag{34}$$

$$\text{at } z = Z_f \quad X_\ell^N = 0$$

$$\frac{dR_\ell^N}{dz} = -\left[\frac{F_R}{P_\ell} + X_\ell^N\right] R_\ell^N - \frac{C_\ell^{N-1}}{P_\ell \Delta\tau} \tag{35}$$

$$\text{at } z = Z_f \quad R_\ell^N = 0$$

$$\frac{dX_s^N}{dz} = \frac{1}{KP_s \Delta\tau} - (X_s^N)^2 \tag{36}$$

$$\text{at } z = 0 \quad X_s^N = 0$$

$$\frac{dR_s^N}{dz} = - X_s^N \; R_s^N - \frac{C_s^{N-1}}{KP_s \Delta\tau} \tag{37}$$

$$\text{at } z = 0 \quad R_s^N = 0$$

After solving equations (34)-(37), the concentration distributions can be obtained by solving the following equations:

$$\frac{dC_\ell^N}{dz} = X_\ell^N \; C_\ell^N + R_\ell^N \tag{38}$$

$$\frac{dC_s^N}{dz} = X_s^N \; C_s^N + R_s^N \tag{39}$$

Calculation of Initial Condition

In order to solve equations (22), (24), (35) and (37), temperature and concentration distributions from the previous time step are needed. This necessitates initial distributions for both the temperature and concentration at the onset of solidification. For the present case, we will assume that no mass diffusion occurs prior to freezing. Thus, the concentration distribution is taken to be

$$C_\ell(z, \tau) = 1$$

throughout the liquid, up until solidification starts.

Since the initial temperature, Θ_0, may not initially be equal to the melting temperature, Θ_m, such an assumption may not be made. We must therefore derive an equation for the temperature as a function of

position and time, which is appropriate to the specific cooling at the upper and lower surfaces. The governing equation [6] for this is

$$\frac{\partial \Theta_\ell}{\partial \tau} = \frac{\partial^2 \Theta_\ell}{\partial z^2} \tag{40}$$

with boundary conditions

$$\frac{\partial \Theta_\ell}{\partial z} = B_1(\Theta_\ell - 1) \quad \text{at } z = 0 \tag{41}$$

$$\frac{\partial \Theta_\ell}{\partial z} = - B_2(\Theta_\ell + \Psi) \quad \text{at } z = 1 \tag{42}$$

and with initial conditions $\Theta_\ell = 0$ at $\tau = 0$. The solution is derived using separation of variables. The solution of the homogenous part takes the form

$$\Theta_\ell (z, \tau) = Z(z)T(\tau)$$

then

$$ZT' = Z''T$$

or

$$\frac{T'}{T} = \frac{Z''}{Z} = - \lambda^2$$

$$\frac{dT}{d\tau} = -\lambda^2 T \qquad \frac{d^2Z}{dz^2} = -\lambda^2 Z$$

$$T = A_1 \exp(-\lambda^2 \tau) \qquad Z = A_2 \sin(\lambda z) + A_3 \cos(\lambda z)$$

and

$$\Theta_\ell = [A_2 \sin(\lambda z) + A_3 \cos(\lambda z)] \exp(-\lambda^2 \tau) \tag{43}$$

$$\frac{\partial \Theta_\ell}{\partial z} = \lambda [A_2 \cos(\lambda z) - A_3 \sin(\lambda z)] \exp(-\lambda^2 \tau) \tag{44}$$

at z = 0

$$\frac{\partial \Theta_\ell}{\partial z} = B_1 \Theta_\ell$$

$$\lambda A_2 \exp(-\lambda^2 \tau) = B_1 A_3 \exp(-\lambda^2 \tau)$$

$$A_2 = \frac{B_1}{\lambda} A_3 \tag{45}$$

at z = 1

$$\frac{\partial \Theta_\ell}{\partial z} = - B_2 \Theta_\ell$$

$$\lambda [A_2 \cos(\lambda) - A_3 \sin(\lambda)] \exp(-\lambda^2 \tau) = - B_2 [A_2 \sin(\lambda) + A_3 \cos(\lambda)] \exp(-\lambda^2 \tau)$$

using (45)

$$B_1A_3\cos(\lambda) - \lambda A_3\sin(\lambda) = - B_2 \left[\frac{B_1A_3}{\lambda} \sin(\lambda) + A_3\cos(\lambda) \right]$$

$$(B_1 + B_2)\cos(\lambda) = \left[\frac{\lambda^2 - B_1B_2}{\lambda} \sin(\lambda) \right]$$

$$\tan(\lambda_N) = \frac{\lambda_N(B_1 + B_2)}{\lambda_N^2 - B_1B_2} \tag{46}$$

So the solution of the homogenous part is

$$\Theta_\ell(z, \tau) = \sum_{N=1}^{\infty} A_N \left[\frac{B_1}{\lambda_N} \sin(\lambda_N z) + \cos(\lambda_N z) \right] \exp(-\lambda_N^2 \tau) \tag{47}$$

Where the eigenvalues, λ_N, are determined from (46).

For the non-homogenous part, assume the solution takes the form

$$\Theta_p = \alpha + \beta z$$

Then, using (41) and (42) we get

$$\beta = B_1(\alpha - 1)$$

and

$$\beta = - B_2(\alpha + \beta + \Psi)$$

combining and solving for α,

$$\alpha = \frac{B_1(1 + B_2) - B_2\Psi}{B_1(1 + B_2) + B_2}$$

Now for the total solution we have

$$\Theta_\ell(z, \tau) = \alpha + \beta z + \sum_{N=1}^{\infty} A_N \left[\frac{B_1}{\lambda_N} \sin(\lambda_N z) + \cos(\lambda_N z) \right] \exp(-\lambda_N^2 \tau)$$

Now using the initial condition

$$\Theta_\ell = 0 \quad \text{at } \tau = 0$$

we can solve for the A_N

$$0 = \alpha + \beta z + \sum_{N=1}^{\infty} A_N \left[\frac{B_1}{\lambda_N} \sin(\lambda_N z) + \cos(\lambda_N z) \right]$$

$$- \alpha - \beta z = \sum_{N=1}^{\infty} A_N E_N(z)$$

$$A_N = \frac{\int_0^1 (-\alpha - \beta z) E_N(z) dz}{\int_0^1 E_N^2(z) dz}$$

$$A_N = \frac{-2\lambda_N \left\{ \left[\alpha + \beta \left(1 + \frac{B_1}{\lambda_N^2} \right) \right] + \left[\frac{\beta}{2\lambda_N} (1 - B_1) - \frac{\alpha B_1}{\lambda_N} \right] \cos(\lambda_N) + \frac{(\alpha B_1 - \beta)}{\lambda_N} \right\}}{\left[B_1^2 + \lambda_N^2 + \tfrac{1}{2} \left(\frac{\lambda_N^2 - B_1^2}{\lambda_N^2} \right) \sin(2\lambda_N) + 2B_1 \sin^2(\lambda_N) \right]}$$

Now, to calculate the distribution for the first state, N = 0, we must find $\tau = \tau_{sol}$ such that the temperature at z = 0, is equal to the melting temperature, θ_m. The initial temperature distribution is then equal to $\theta(z,\tau_{sol})$.

CHAPTER III

SOLUTION AND RESULTS

Numerical Method

In order to solve for the temperature and concentration distributions in both the liquid and solid phases, equations (21)-(24) and (34)-(37) must first be solved. These equations comprise of a set of coupled, nonlinear ordinary differential equations with their proper boundary conditions. Such a set of boundary value problems are most suitably solved with a Runge-Kutta-Fehlberg [10] integrator. For the present problem, a RK7(8) was used. Before integrating these equations, a new interface position, S^N, and concentration, C_ℓ^N, must be assumed. Once these equations are solved, the temperature and concentration gradients at the interface may be obtained from equations (25), (26), (38) and (39). The conservation of energy (20) and mass (29) equations at the interface are then used to check these results. If the initial guess on S^N and C_ℓ^N was in error, these equations will not be satisfied. A better estimate for the correct values of S^N and C_ℓ^N can be obtained from these equations through a Newton-Rhapson method. This process of evaluating the temperature and concentration gradients and reestimating the interface position and concentration is repeated until convergence to the correct values occurs. Now, equations (25), (26), (38) and (39) can be integrated for the temperature and concentration profiles from the interface to the lower surface for the solid and from the interface to the upper surface for

the liquid. The time is then advanced by one time step, $\Delta\tau$, and the process repeated for the new interface position.

This method (Antar [2]) gave satisfactory results down to a Lewis number, P_s, of order 10^{-4}. At lower Lewis numbers overflow problems occurred due to the stiffness of equation (36). This can easily be seen by using the following values as an example:

$$P_s = 10^{-5}$$

$$K = 2.7$$

$$\Delta\tau = 1$$

To demonstrate the problem, we will use a fourth order Runge-Kutta technique as outlined in ref [4], and the above values with the boundary condition of zero,

if

$$y' = f(z,y) \text{ with } a \leq z \leq b$$

$$y(a) = \text{boundary value}$$

$$h = \frac{b - a}{N} \quad \text{where } N = \text{number of intervals}$$

then an approximate solution to y is w, found in the following manner:

$$w_0 = \text{boundary value}$$

$$k_1 = hf(x_i, w_i)$$

$$k_2 = hf(x_i + \frac{h}{2} , w_i + \frac{1}{2}k_1)$$

$$k_3 = hf(x_i + \frac{h}{2} , w_i + \frac{1}{2}k_2)$$

$$k_4 = hf(x_{i+1} , w_i + k_3)$$

$$w_{i+1} = \frac{1}{6} (k_1 + 2k_2 + 2k_3 + k_4)$$

for each i = 0, . . . , N - 1.

Applying this to equation (36) with 50 intervals we arrive at the following values:

For i = 0

$$k_1 = +7.407 \times 10^2$$

$$k_2 = -2.003 \times 10^3$$

$$k_3 = -1.931 \times 10^4$$

$$k_4 = -7.460 \times 10^6$$

and

$$w_1 = -1.250 \times 10^6$$

For i = 1

$$k_1 = -3.127 \times 10^{10}$$

$$k_2 = -4.889 \times 10^{18}$$

$$k_3 = -1.195 \times 10^{35}$$

$$k_4 = -2.865 \times 10^{68}$$

The calculation for k_4 causes overflow on the VAX 11/780, which has an upper bound of order 10^{38}.

Analytical Method

Inspection of equations (21) and (34) reveals them to be of the following general type:

$$\frac{dy}{dz} = A - By - y^2$$

There exists a closed form solution [16] for this type of equation. Finding closed form solutions avoids the use of numerical integrators, therefore rendering the problem of stiffness more manageable. The solution is found by using the transformation

$$y = \frac{u'}{u}$$

The equations then take the form

$$u'' + Bu' - Au = 0$$

whose solution is found in the following manner.

The characteristic equation is

$$r^2 + Br - A = 0$$

$$r_{1,2} = \frac{1}{2}\left(-B \pm \sqrt{B^2 + 4A}\right)$$

$$u = C_1 \exp(r_1 z) + C_2 \exp(r_2 z)$$

then

$$y = \frac{r_1 \exp(r_1 z) + C r_2 \exp(r_2 z)}{\exp(r_1 z) + C \exp(r_2 z)}$$

where

$$C = -\frac{(r_1 - y)}{(r_2 - y)} \exp((r_1 - r_2) z)$$

Similarly, equations (23) and (36) have the form

$$\frac{dy}{dz} = A - y^2$$

and can be solved using the same transformation

$$y = \frac{u'}{u}$$

yielding

$$u'' = Au$$

$$u = C_1 \exp(\sqrt{A} z) + C_2 \exp(-\sqrt{A} z)$$

$$y = \sqrt{A}\ \left[\ \frac{\exp(\sqrt{A}z) - C\exp(-\sqrt{A}z)}{\exp(\sqrt{A}z) + C\exp(-\sqrt{A}z)}\ \right]$$

with

$$C = \left[\ \frac{\sqrt{A} - y}{\sqrt{A} + y}\ \right] \exp(2\sqrt{A}z)$$

Equations (22), (24-26), (35), (37-39) are of a more complicated type

$$\frac{dy}{dz} = -F(z)y - G(z)$$

but can be easily solved using the Variation of Parameters technique [9].

$$y = \exp\left(-\int_{z_i}^{z} F(z)dz\right)\left[\ C - \int_{z_i}^{z} G(z')\exp\left(\int_{z_i}^{z'} F(z)dz\right)dz'\ \right]$$

Equations (22), (24), (35) and (37) contain functions whose values are known only at certain points, requiring quadrature evaluations to determine their solutions. These techniques, though, are known to be highly stable, allowing solutions to be obtained at lower Lewis numbers. The same iterative technique as described earlier is used to determine the interface position and the temperature and concentration profiles at each time step.

Now the solutions of equations (21)-(24) and (34)-(37) are:

$$Y_{\ell}^{N} = \frac{r_1\exp(r_1z) + C_1r_2\exp(r_2z)}{\exp(r_1z) + C_1\exp(r_2z)} \qquad (48)$$

$$r_{1,2} = \frac{1}{2}\left[- F_R \pm \sqrt{F_R^2 + \frac{4}{\Delta\tau}} \right]$$

$$C_1 = - \frac{(r_1 - B_2)}{(r_2 - B_2)} \exp((r_1 - r_2) z_f)$$

$$Z_\ell^N = \exp(-\int_z^{z_f} (F_R + Y_\ell^N) dz) \left[C_2 - \int_z^{z_f} \frac{\Theta_\ell^{N-1}}{\Delta\tau} \exp(\int_{z'}^{z_f} (F_R + Y_\ell^N) dz) dz' \right] \quad (49)$$

$$C_2 = - B_2 \Psi$$

$$Y_s^N = \delta \left[\frac{\exp(\delta z) - C_5 \exp(-\delta z)}{\exp(\delta z) + C_5 \exp(-\delta z)} \right] \quad (50)$$

$$C_5 = \frac{\delta K - B_1}{\delta K + B_1}$$

$$\delta = \frac{1}{\sqrt{K\Delta\tau}}$$

$$Z_s^N = \exp(-\int_0^z Y_s^N dz) \left[C_6 - \int_0^z \frac{\Theta_s^{N-1}}{K\Delta\tau} \exp(\int_0^{z'} Y_s^N dz) dz' \right] \quad (51)$$

$$C_6 = \frac{- B_1}{\Lambda}$$

$$X_\ell^N = \frac{r_1 \exp(r_1 z) + C_3 r_2 \exp(r_2 z)}{\exp(r_1 z) + C_3 \exp(r_2 z)} \quad (52)$$

$$r_{1,2} = \frac{1}{2}\left[- \frac{F_R}{P_\ell} \pm \sqrt{\left(\frac{F_R}{P_\ell}\right)^2 + \frac{4}{P_\ell \Delta\tau}} \right]$$

$$C_3 = - \frac{r_1}{r_2} \exp((r_1 - r_2) z_f)$$

$$R_\ell^N = \exp\left(- \int_z^{z_f} \left(\frac{F_R}{P_\ell} + X_\ell^N\right) dz\right) \int_z^{z_f} \frac{C_\ell^{N-1}}{P_\ell \Delta\tau} \exp\left(- \int_{z'}^{z_f} \left(\frac{F_R}{P_\ell} + X_\ell^N\right) dz\right) dz' \tag{53}$$

$$X_s^N = \frac{\delta}{\sqrt{P_s}} \tanh\left(\frac{\delta z}{\sqrt{P_s}}\right) \tag{54}$$

$$R_s^N = \left(\frac{-1}{\cosh\left(\frac{\delta z}{\sqrt{P_s}}\right)}\right) \int_0^z \frac{C_s^{N-1}}{K P_s \Delta\tau} \cosh\left(\frac{\delta z}{\sqrt{P_s}}\right) dz \tag{55}$$

Now the solution to equations (25), (26), (38) and (39) can be found using the Variation of Parameters technique [9].

$$\Theta_\ell^N(z) = \exp\left(\int_{z_i}^{z} Y_\ell^N dz\right) \left[C_9 + \int_{z_i}^{z} Z_\ell^N \exp\left(- \int_{z_i}^{z} Y_\ell^N dz\right) dz' \right] \tag{56}$$

$$\Theta_s^N(z) = \exp\left(\int_{z_i}^{z} Y_s^N dz\right) \left[C_{10} + \int_{z_i}^{z} Z_s^N \exp\left(- \int_{z_i}^{z} Y_s^N dz\right) dz' \right] \tag{57}$$

$$C_\ell^N(z) = \exp\left(\int_{z_i}^{z} X_\ell^N\right) \left[C_{11} + \int_{z_i}^{z} R_\ell^N \exp\left(- \int_{z_i}^{z'} X_\ell^N dz\right) dz' \right] \tag{58}$$

$$C_s^N(z) = \exp\left(\int_{z_i}^{z} X_s^N\right) \left[C_{12} + \int_{z_i}^{z} R_s^N \exp\left(- \int_{z_i}^{z'} X_s^N dz\right) dz' \right] \tag{59}$$

The constants, C_9 and C_{11}, represent the temperature and concentration of the liquid at the interface. The constants, C_{10} and C_{12}, represent the temperature and concentration of the solid at the interface. C_9 and C_{10} must be equal. Since only the conditions at the interface are known, the integrations in equation (56) and (58) are performed from the interface up, and, in equations (57) and (59), from the interface down.

Asymptotic approximations were used whenever possible to reduce the chance of overflow errors. For example, equation (50) is evaluated as

$$Y_s^N = \delta$$

whenever

$$\delta z \geq 60$$

Also, exponents were combined as much as possible. In equation (59), for example,

$$\int_{z_i}^{z} X_s^N \, dz$$

was evaluated first, then treated as a constant so that it could be carried within the integral and added to the exponent before the exponents are evaluated.

Many of the integrals could not be solved exactly because they contain the concentration or temperature functions whose values are known only at certain points. They were therefore solved using a 15

point Gauss-Legendre quadrature, with maximum interval size of 0.1, and a cubic spline interpolation [4] between the known points.

$$\int_a^b F(x)dx = \frac{(b-a)}{2} \sum_{i=1}^{15} w_i F\left(\frac{r_i(b-a)+b+a}{2}\right)$$

The roots and weights (r_i, w_i) were obtained from Table 2.2 in ref [5].

This method gave good results down to a Lewis number, P_s, of order 10^{-6}. Below this value, problems occur due to the accuracy of the integrator, when applied to equation (59). The error occurs when

$$\int_{z_i}^{z} R_s^N \exp\left(-\int_{z_i}^{z'} X_s^N dz\right)dz' \qquad (60)$$

is evaluated. To demonstrate this, using the functions

$$X_s^N = \frac{\delta}{\sqrt{P_s}} \tanh\left(\frac{\delta z}{\sqrt{P_s}}\right)$$

and

$$R_s^N = \frac{1}{\cosh\left(\frac{\delta z}{\sqrt{P_s}}\right)} \int_0^z \frac{\cosh\left(\frac{\delta z}{\sqrt{P_s}}\right)}{KP_s\Delta\tau} dz$$

$$R_s^N = -\delta \frac{\tanh\left(\frac{\delta z}{\sqrt{P_s}}\right)}{\sqrt{P_s}}$$

we evaluate equation (60) in closed form. Note that these equations are the same as (54) and (55), except for the missing concentration term in (55). The exact solution of (60) then is

$$\operatorname{sech}\left(\frac{\delta}{\sqrt{P_s}}\right) - 1$$

when evaluated from zero to one. For large values of $\delta/\sqrt{P_s}$ the solution approaches the value of -1.0. Evaluating equation (60) numerically, using a 15 point Gauss-Legendre quadrature with 10 intervals, and the following parameters

$$K = 2.7$$

$$P_s = 10^{-7}$$

$$\Delta\tau = 1$$

$$z_i = 0$$

$$z = 1$$

we get the value of -1.36, which is a difference of .36 from the true value. Table 1 lists the results of different interval sizing at different values of P_s.

Table 1

The Effects of Different Interval Sizing on the Accuracy of a Gauss-Legendre Quadrature Technique

Value of P_s	Number of Intervals in Quadrature	Difference from Actual Value
10^{-6}	10	2.33×10^{-2}
10^{-7}	10	3.62×10^{-1}
10^{-7}	100	1.22×10^{-4}
10^{-7}	250	1.30×10^{-7}
10^{-8}	100	3.15×10^{-2}
10^{-8}	250	5.24×10^{-4}
10^{-8}	500	4.60×10^{-6}

Reasonable accuracy is obtained for P_s of order 10^{-7} using 250 intervals. However, combined with a 15 point quadrature formula, this means 3750 function evaluations (actually, equation (55) has an additional integration, requiring 56,250 evaluations), which means a high probability of round-off error occurring during the computations.

Computation Results

As previously discussed, the numerical technique gave good results down to a Lewis number, P_s, of 10^{-4}. Alloys having this high rate of diffusion in its solid phase are rare. For more common alloys, such as lead-tin (Pb-Sn), the Lewis number is of order 10^{-10} [7]. Because of this restriction the analytical technique was derived. With this technique, we were able to get results down to a Lewis number, P_s, of order 10^{-6}. The following parameters, based on the temperature differences

$$T_0 - T_m = 5^o$$

$$T_m - T_1 = 2^o$$

$$T_2 - T_m = 4^o$$

were used in the calculations.

$K = 2.326$ $\qquad$ $B_1 = 1.00$

$M = - 0.22$ $\qquad$ $B_2 = 0.01$

$L = - 27.7$ $\qquad$ $R = 1.00$ or 1.06

$P_\ell = 10^{-2}$ $\qquad$ $P_s = 10^{-4} \rightarrow 10^{-6}$

$\hat{k} = 0.580$ $\qquad$ $\Psi = - 0.14286$

$\Lambda = 2.703$ $\qquad$ $\Delta\tau = 1$

A more realistic liquid Lewis number, P_ℓ, is of order 10^{-4}[8]. Computations were performed at a Lewis number, P_ℓ, of 10^{-2} in order to keep at least the ratio of liquid to solid diffusion rates realistic. Comparison of the two techniques at $P_s = 10^{-4}$ is shown in Figures 3, 4 and 5. The interface position and the temperature and concentration at the interface as a function of time are shown to match excellently. The solid lines represent the analytical solution while the circles represent the numerical solution.

The next series of plots, Figures 6, 7 and 8, show concentration distributions at different Lewis numbers at time step intervals of 25, with the first time step at 25 and the last at 200. The interface position is seen as the vertical lines with the solid phase to the left and the liquid phase to the right. The effects of lower Lewis numbers are very apparent. In Figure 6, at Lewis number 10^{-4}, there is significant diffusion in the solid, while in Figure 8, at Lewis number 10^{-6}, almost no diffusion is noticeable. The only movement is at the lower surface, which has had more time for diffusion to occur.

Figures 9-20 show how the interface, concentration and temperature vary with time and the temperature with interface position at the three Lewis numbers, 10^{-4}, 10^{-5} and 10^{-6}. We can see in Figures 9, 13 and 17, that the velocity of the interface is decreasing as the alloy solidifies. The upward motion of the interface has all but stopped. This is due to equation (7), which determines the melting temperature of the alloy. As seen in the phase diagram, the melting temperature decreases, as concentration increases, to a

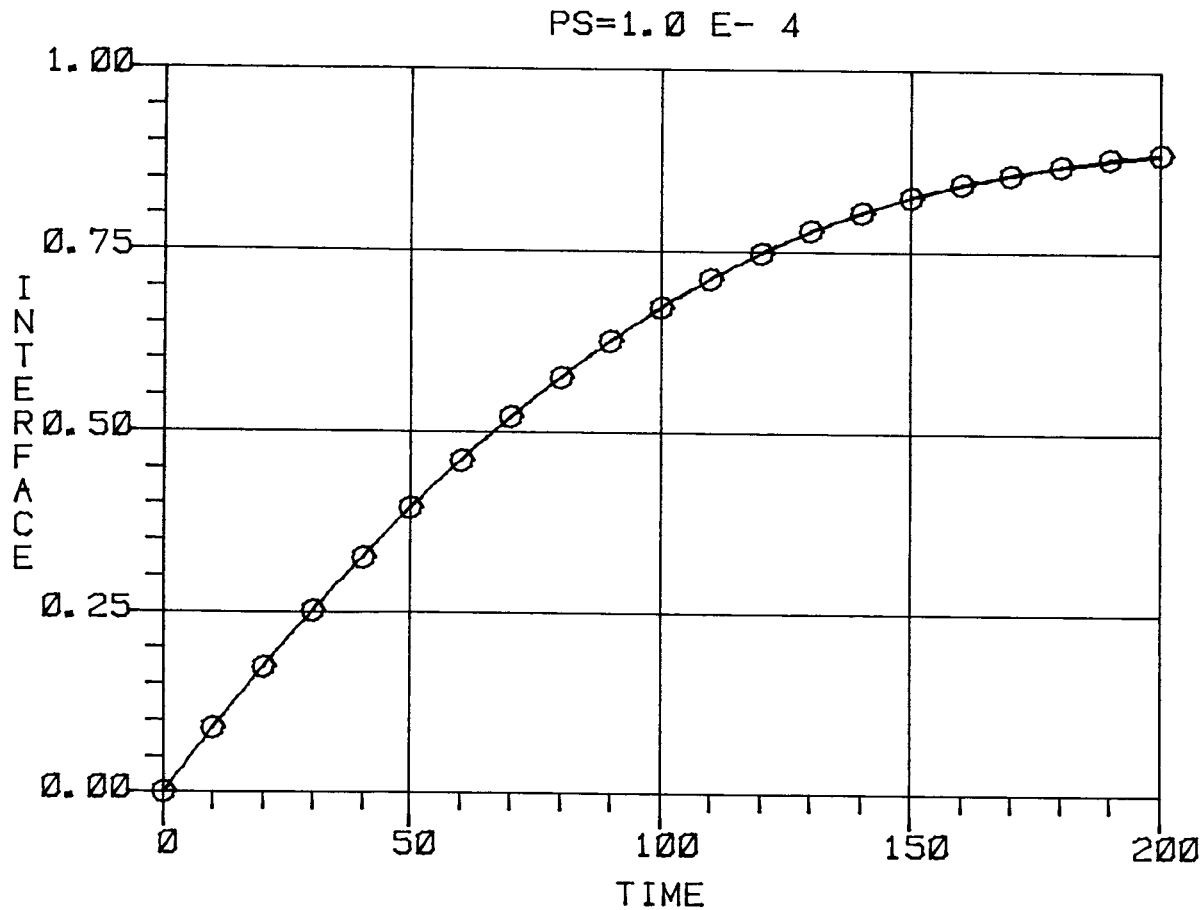

Figure 3. Comparison of interface position vs. time for numerical and analytical techniques. Solid = analytical, Circles = numerical.

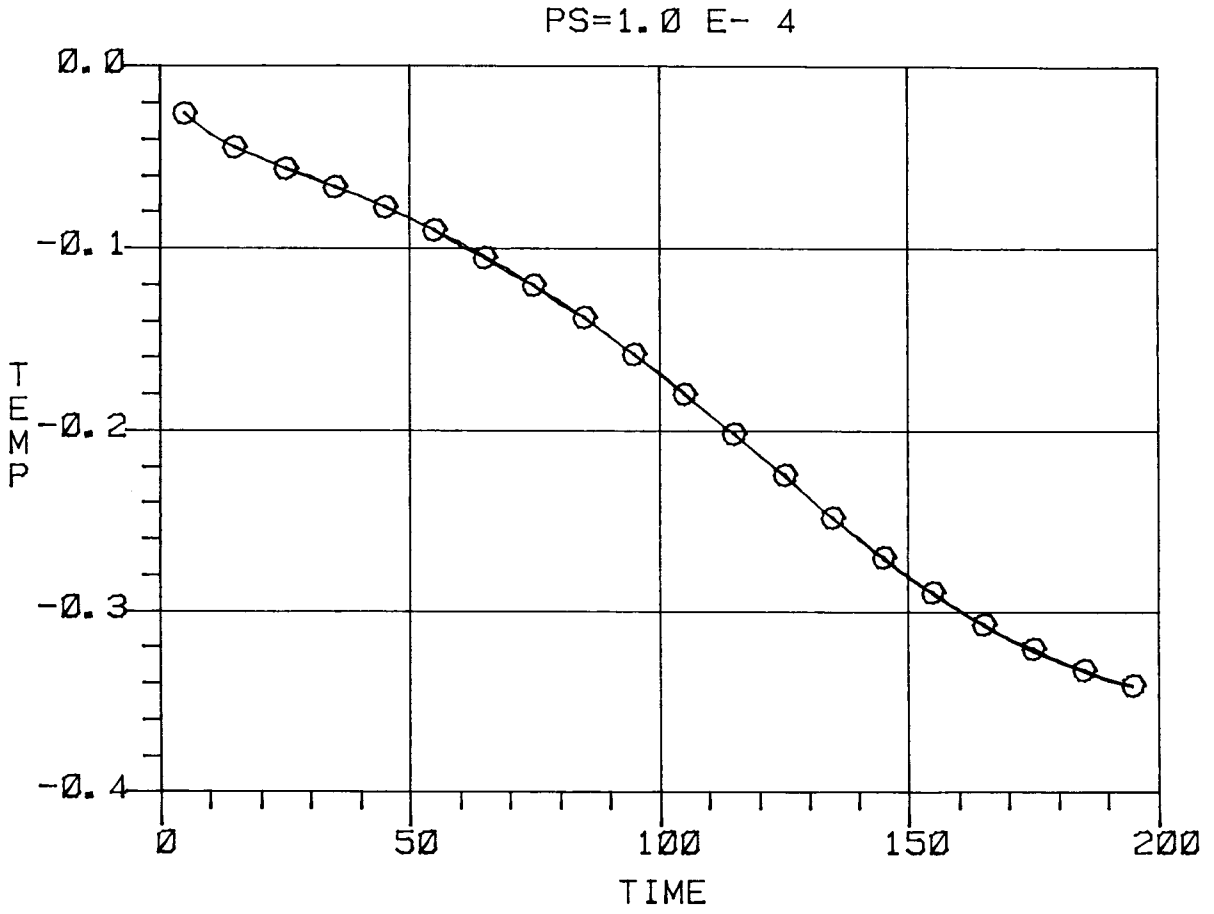

Figure 4. Comparison of temperature vs. time for numerical and analytical techniques. Solid = analytical, Circles = numerical.

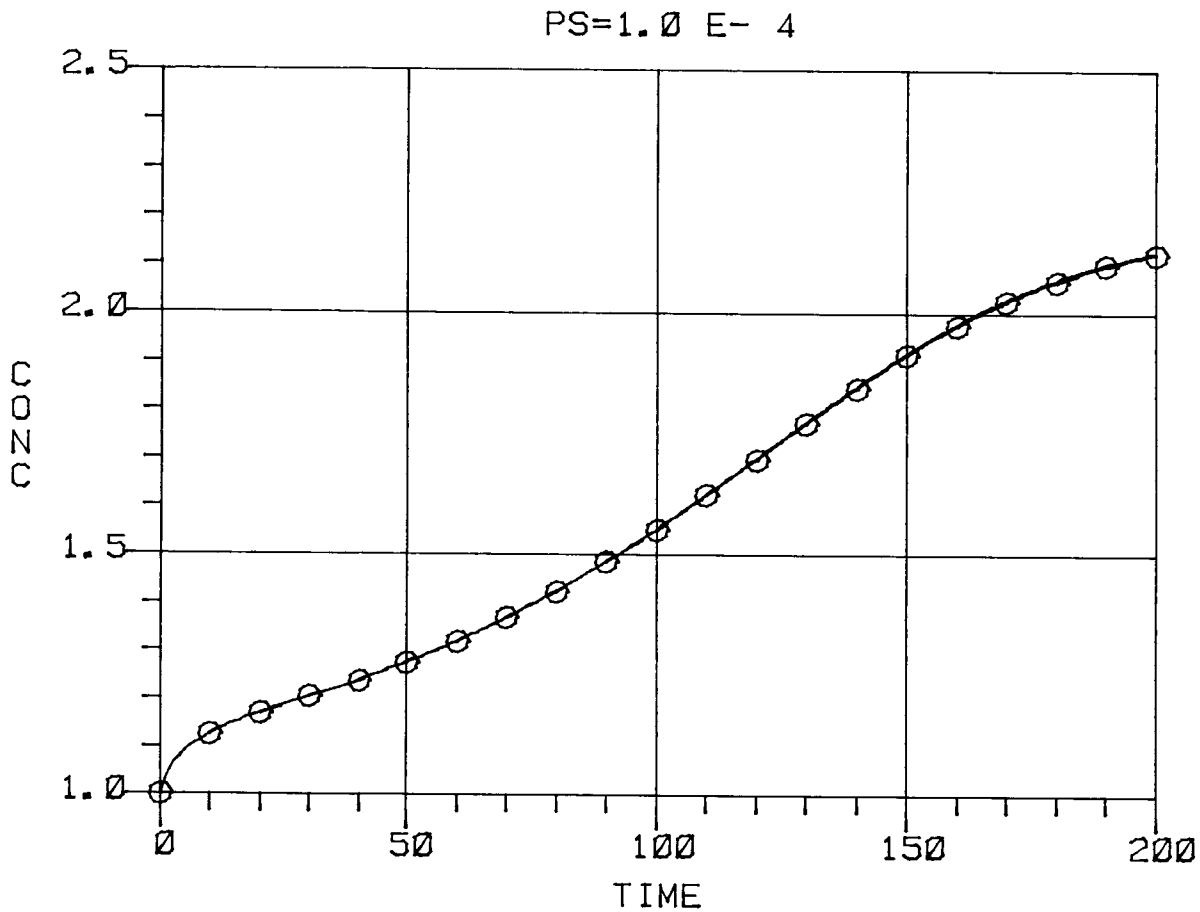

Figure 5. Comparison of concentration vs. time for numerical and analytical techniques. Solid = analytical, Circles = numerical.

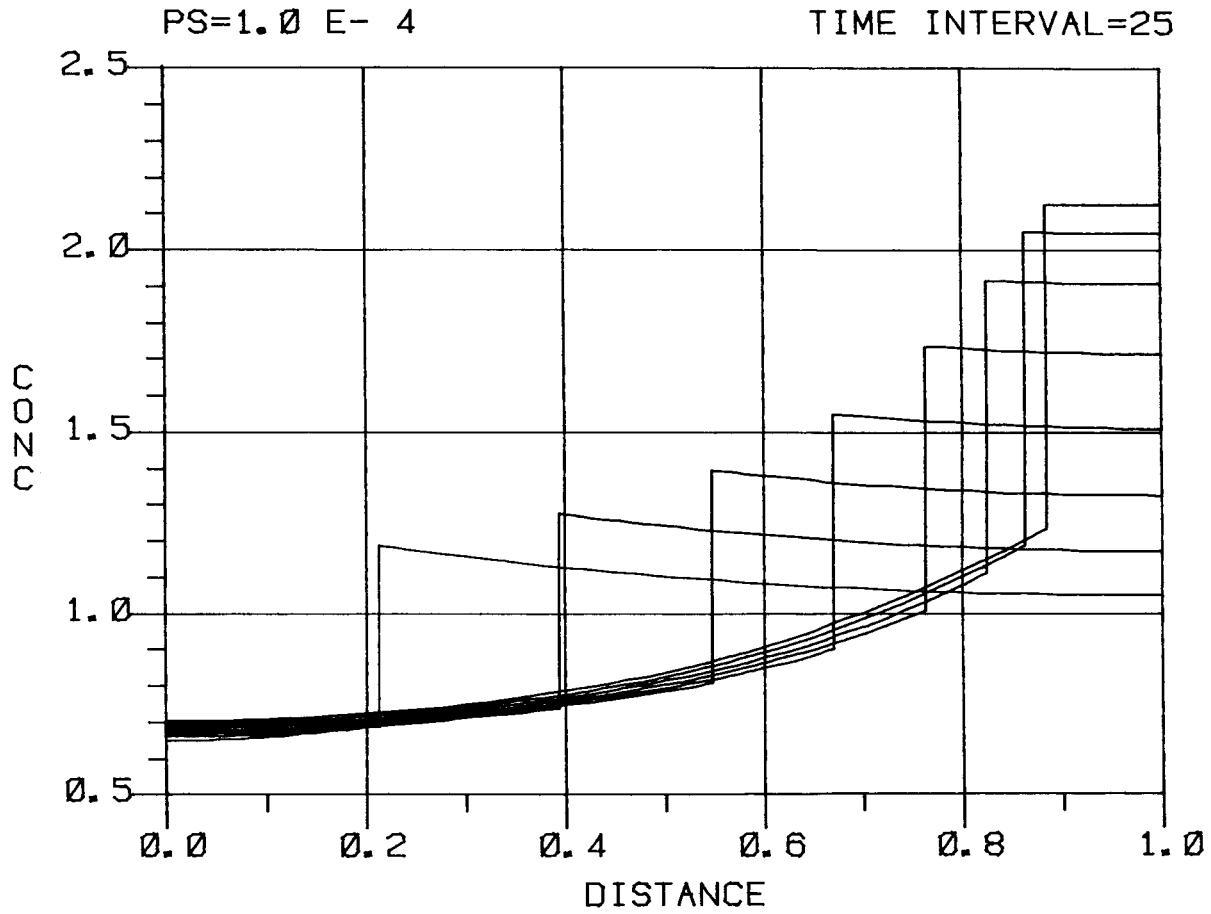

Figure 6. Concentration distributions at $P_s = 10^{-4}$.

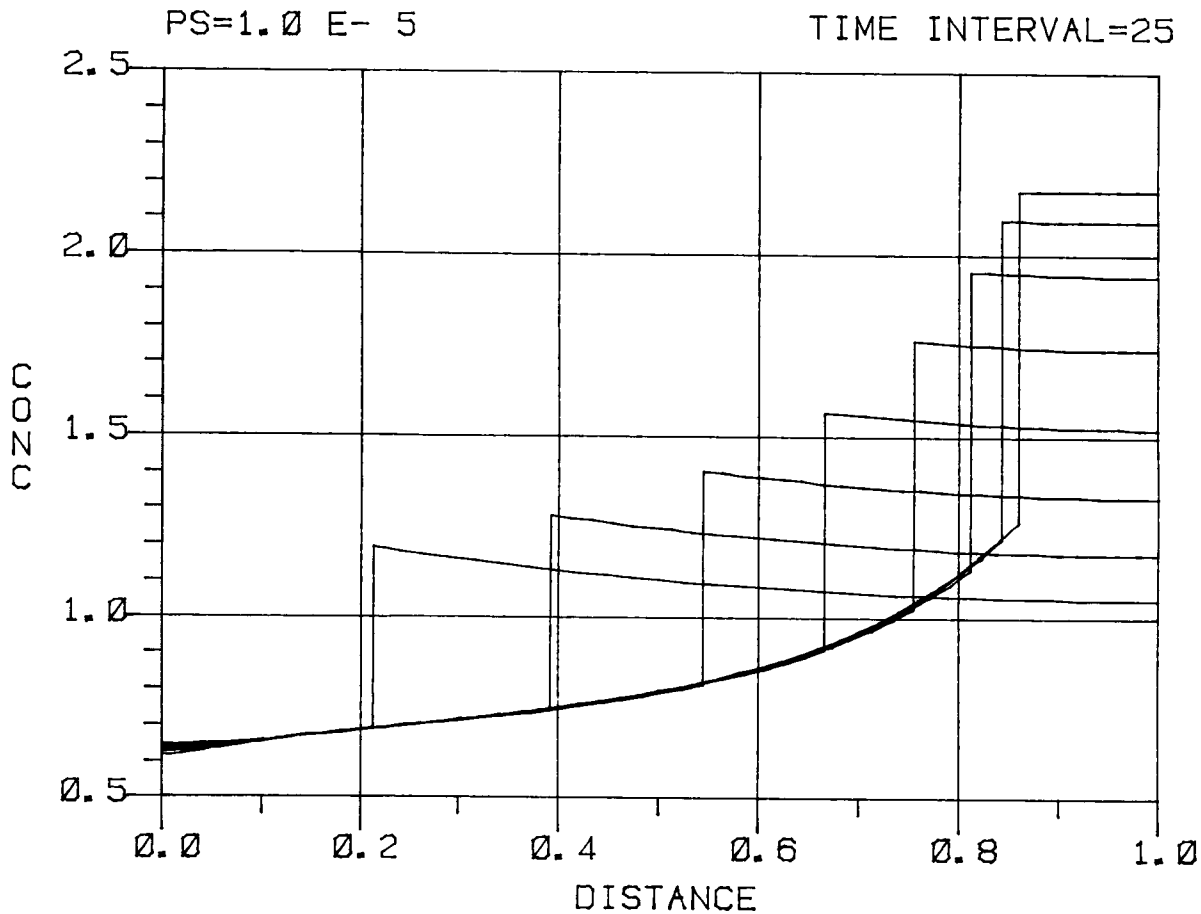

Figure 7. Concentration distributions at $P_s = 10^{-5}$.

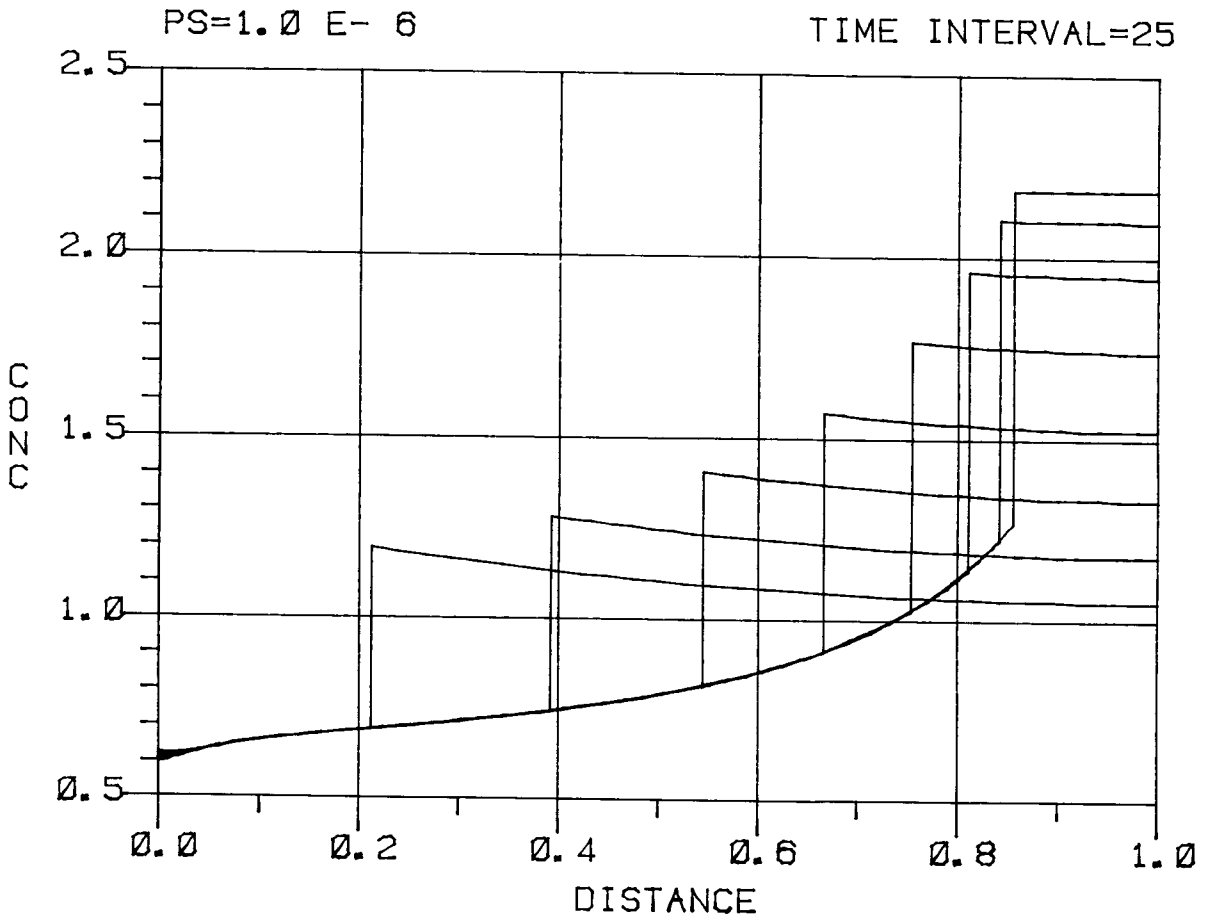

Figure 8. Concentration distributions at $P_s = 10^{-6}$.

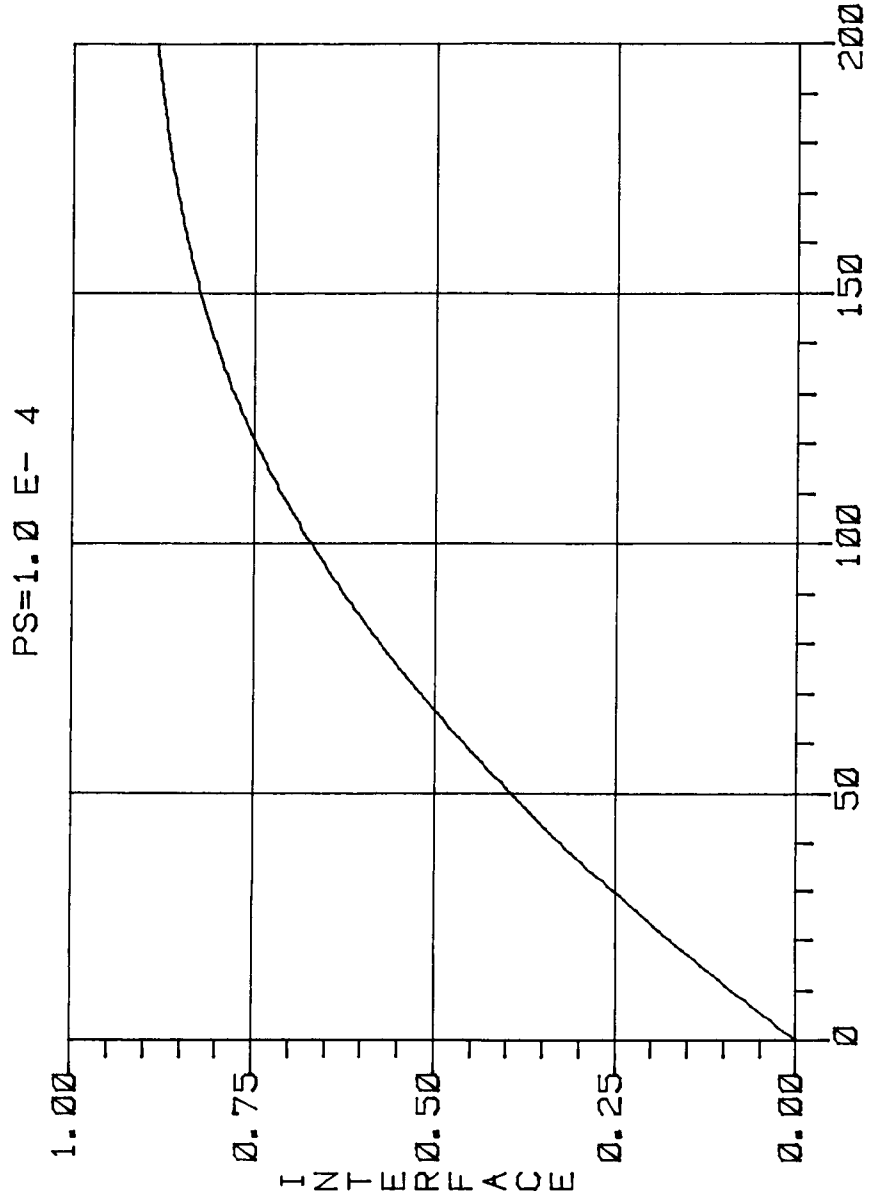

Figure 9. Interface vs. time at $P_s = 10^{-4}$.

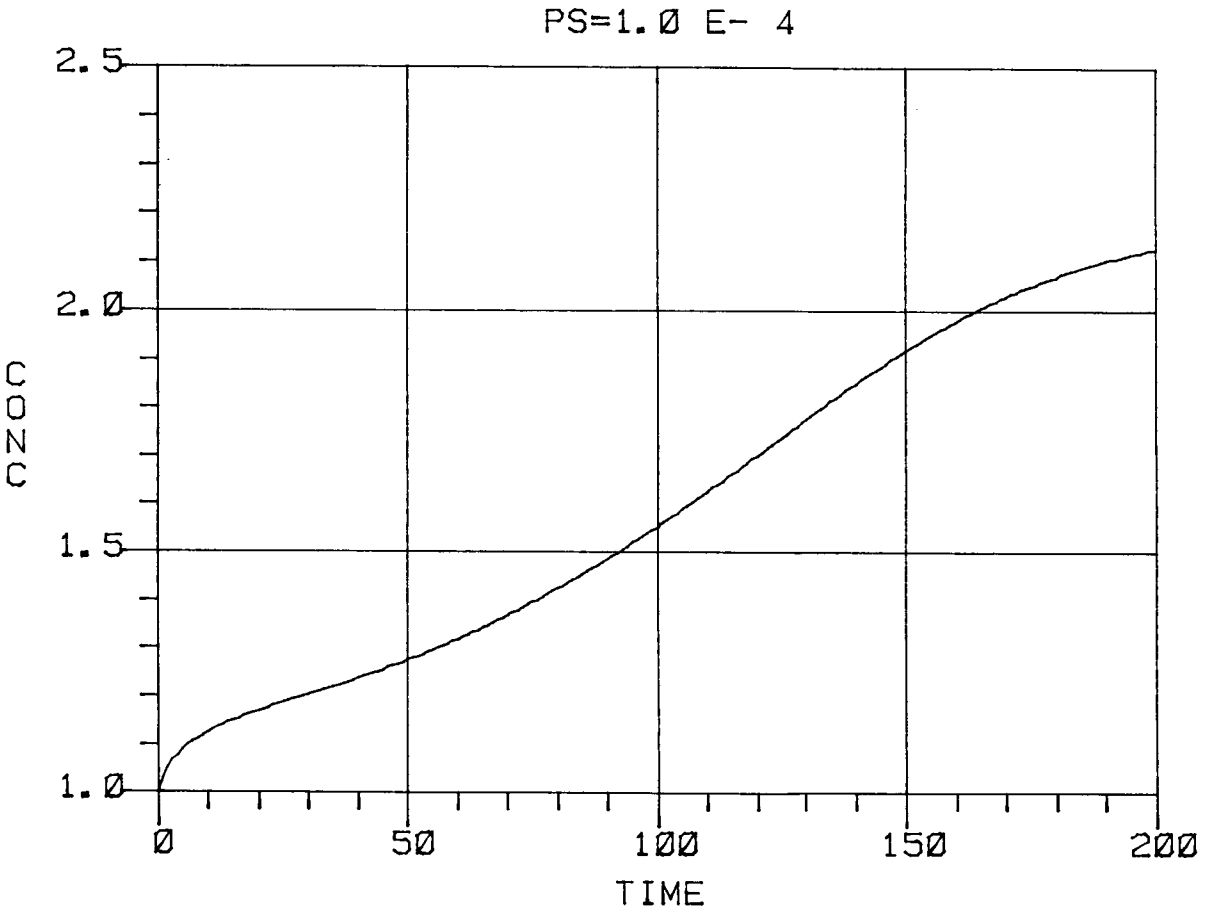

Figure 10. Concentration vs. time at $P_s = 10^{-4}$.

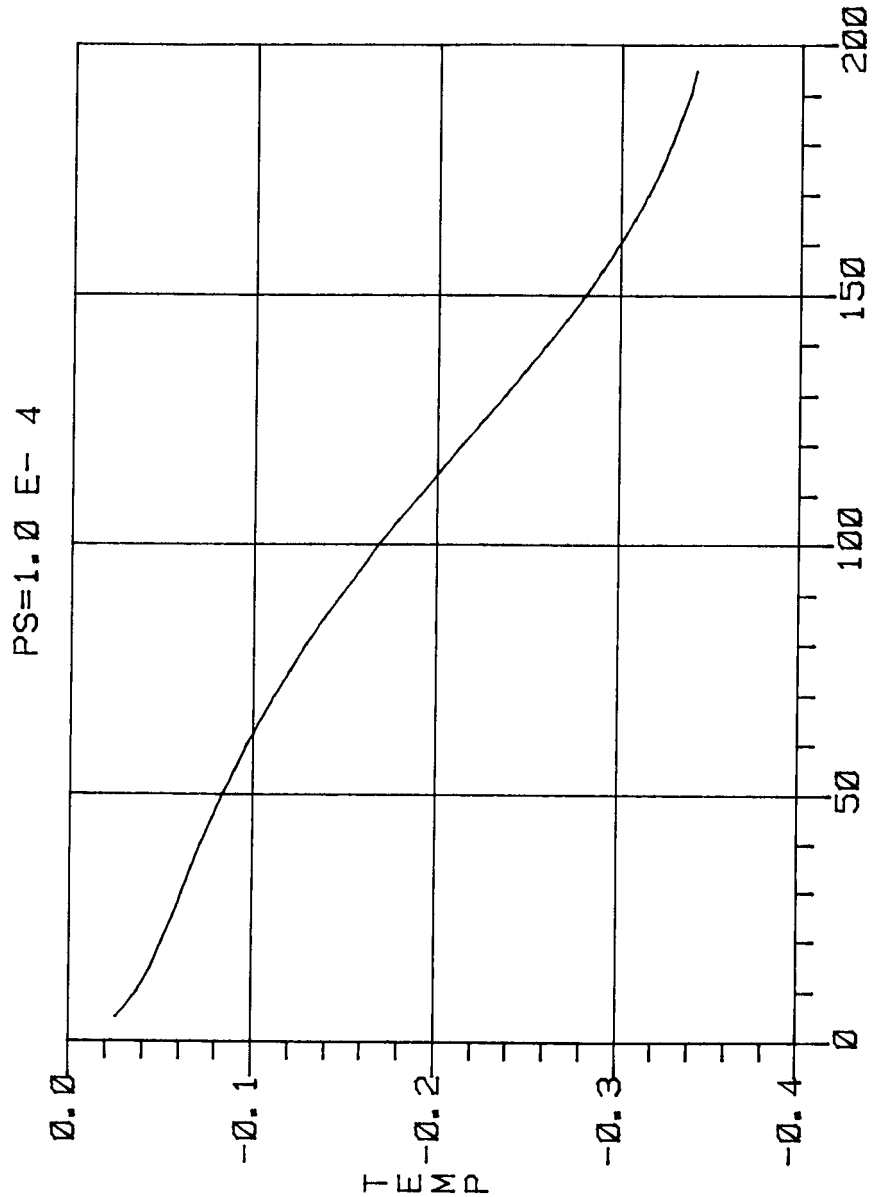

Figure 11. Temperature vs. time at $P_s = 10^{-4}$.

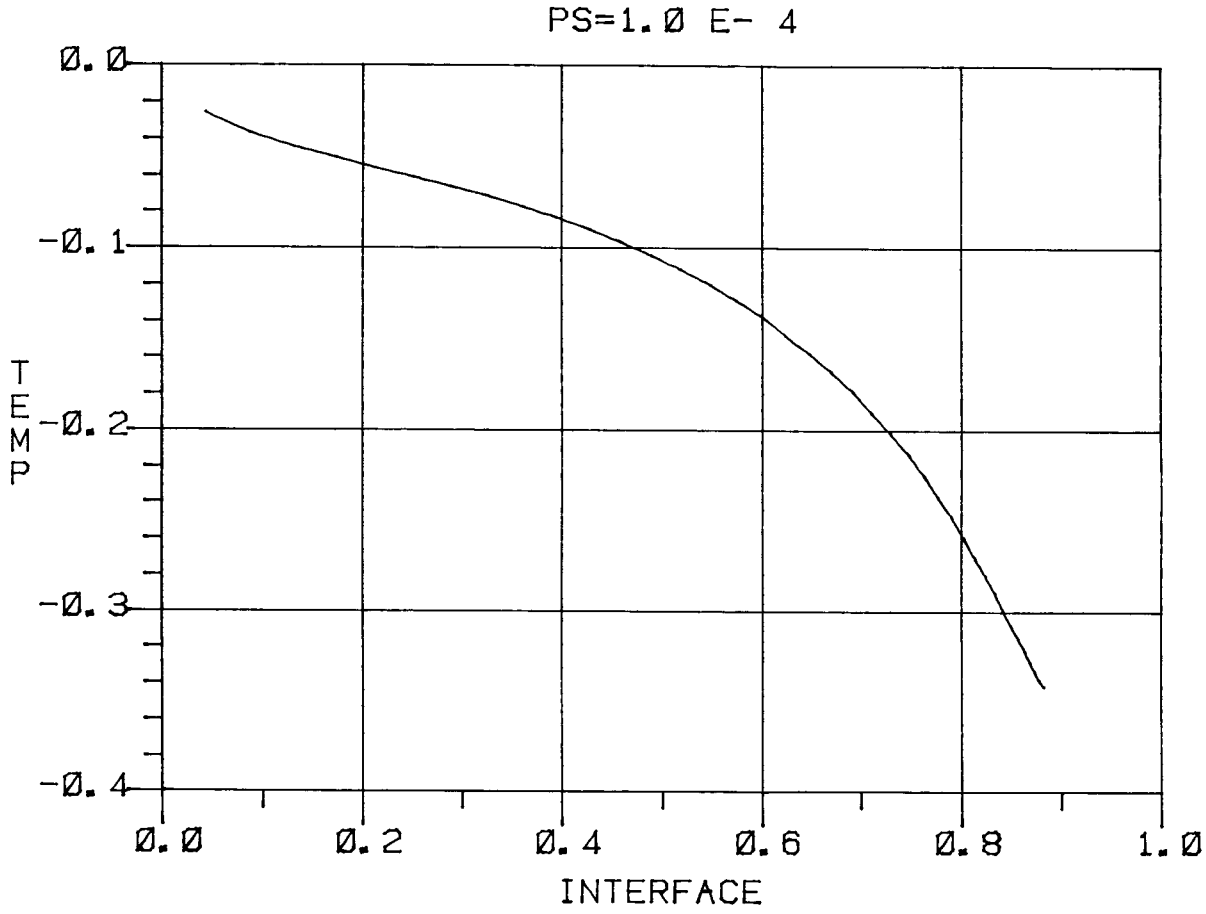

Figure 12. Temperature vs. interface at $P_s = 10^{-4}$.

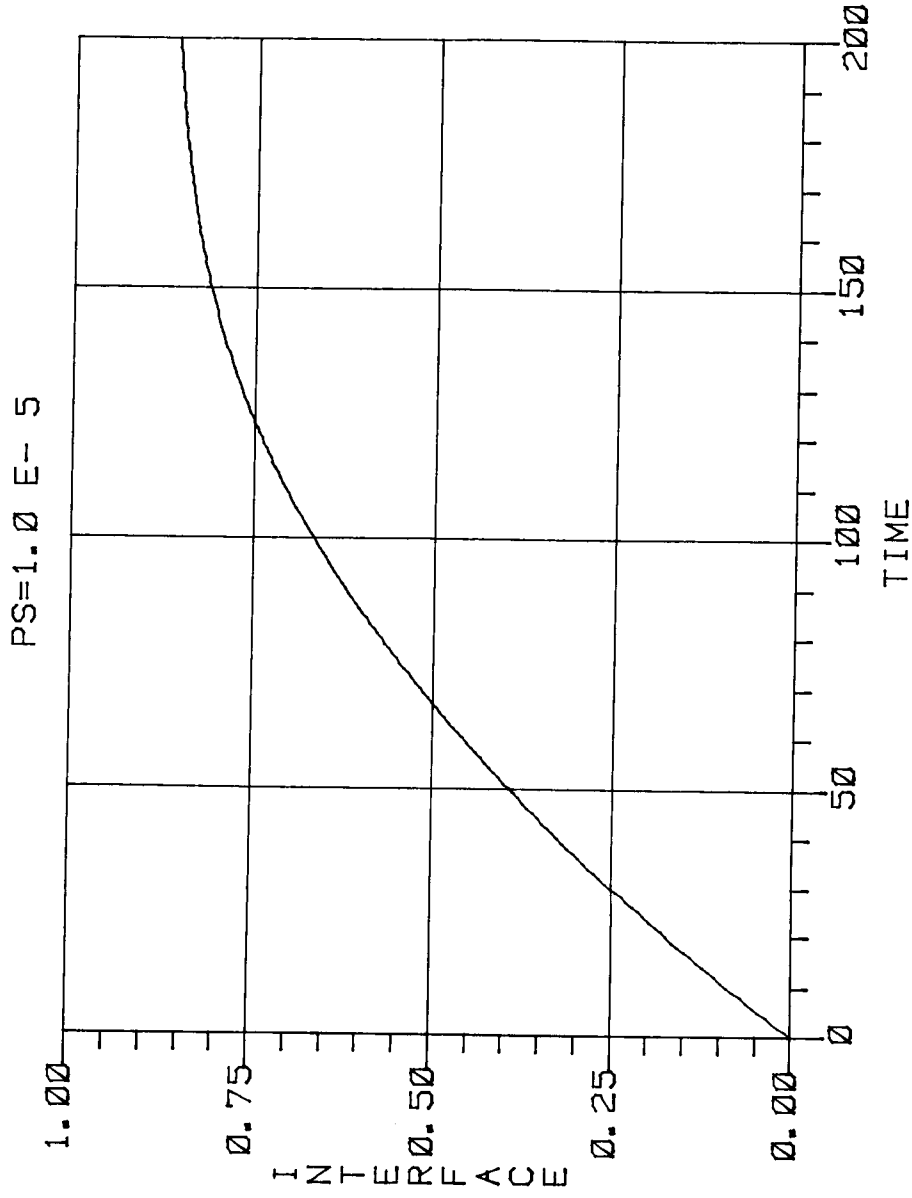

Figure 13. Interface vs. time at $P_s = 10^{-5}$.

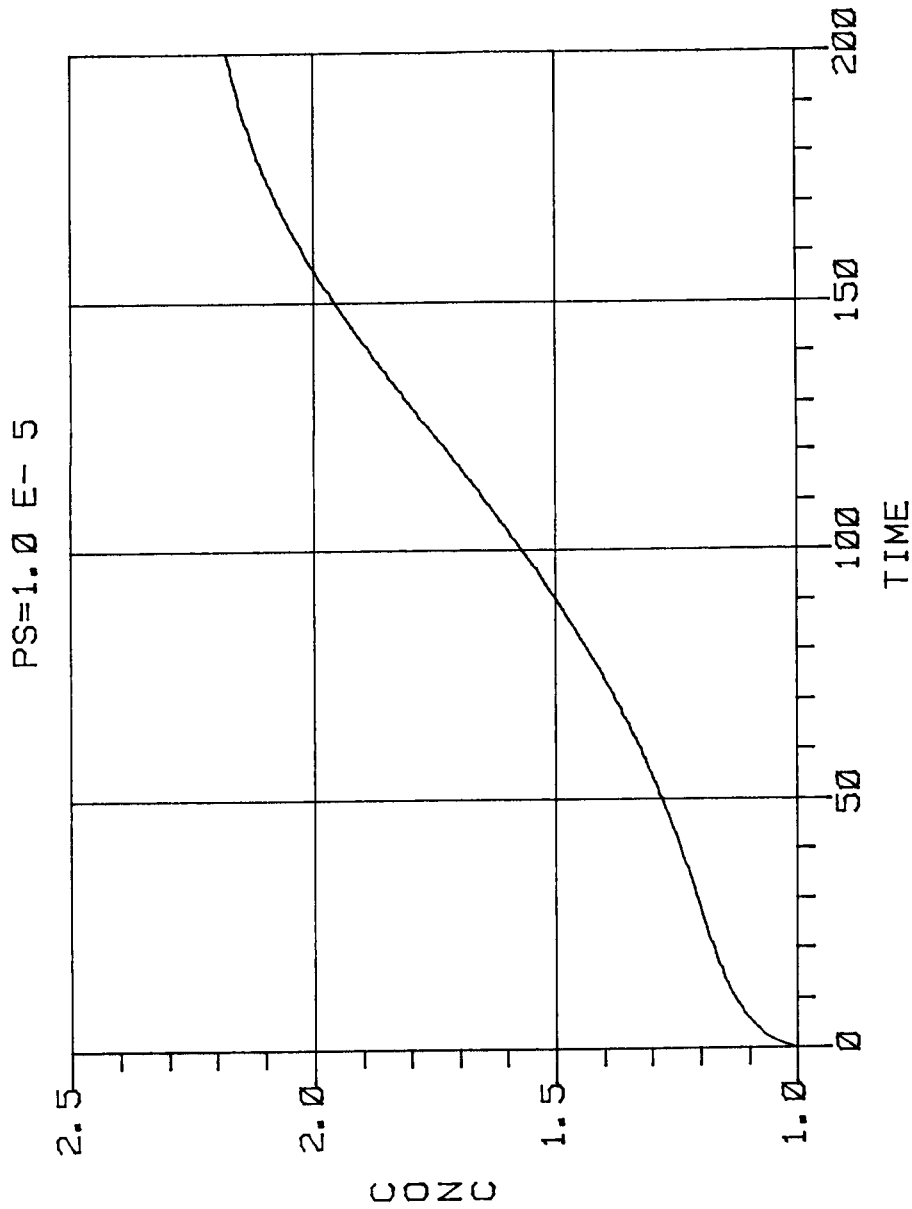

Figure 14. Concentration vs. time at $P_s = 10^{-5}$.

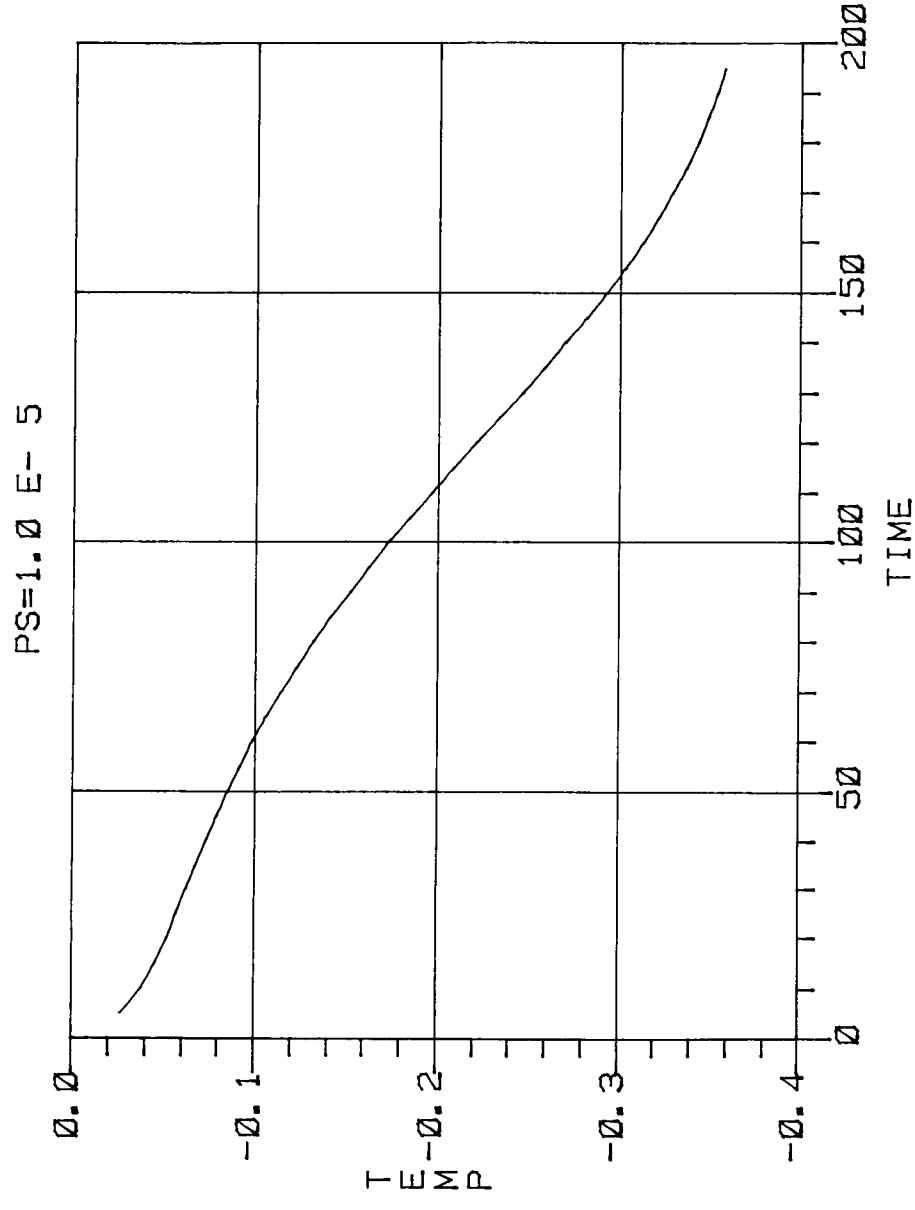

Figure 15. Temperature vs. time at $P_s = 10^{-5}$.

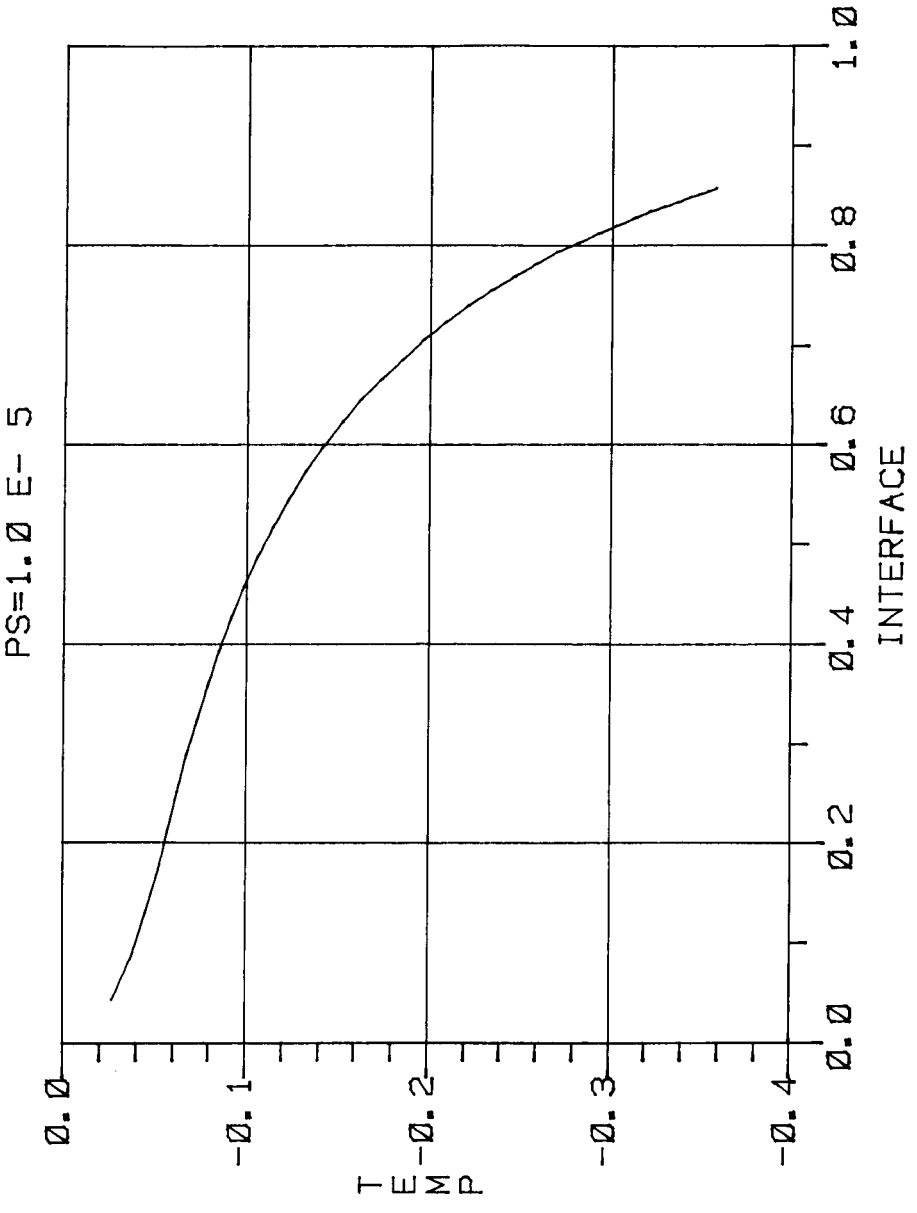

Figure 16. Temperature vs. interface at $P_s = 10^{-5}$.

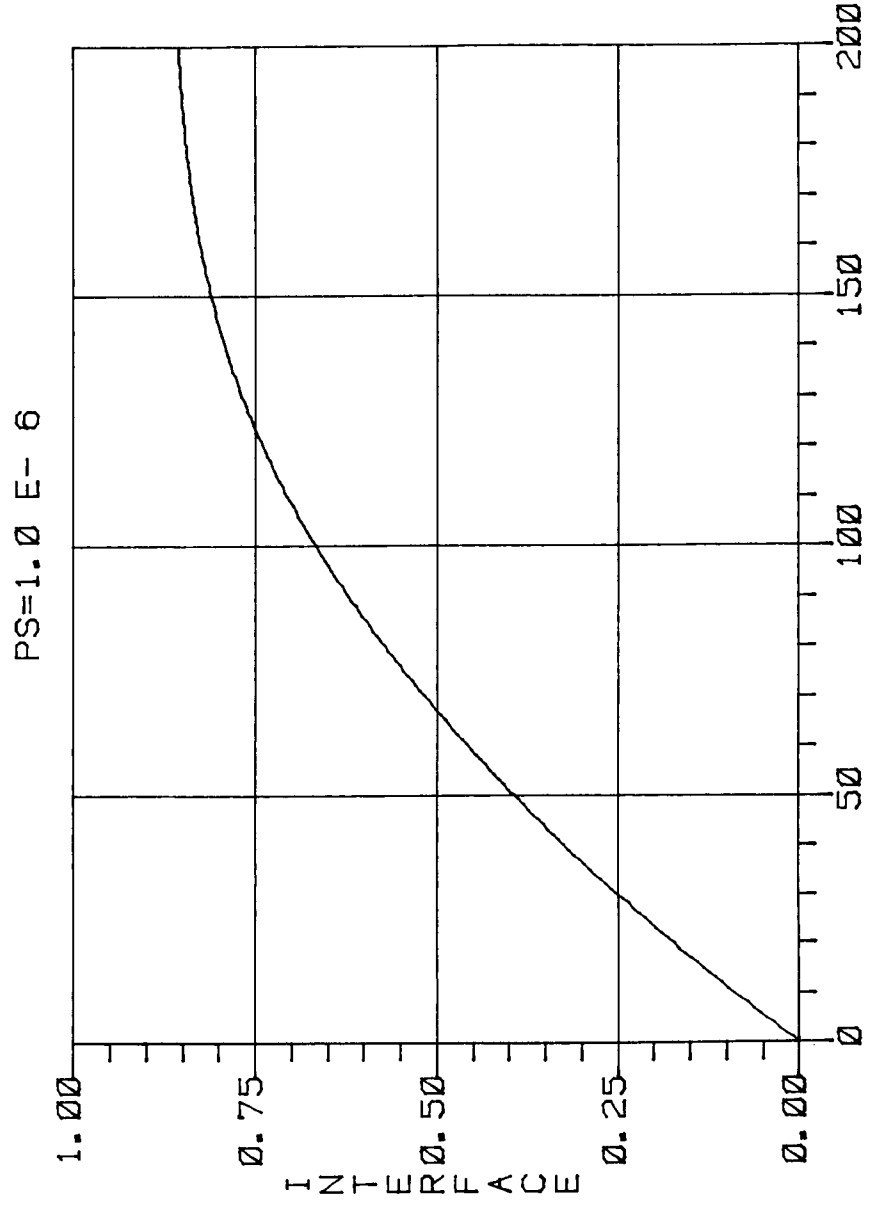

Figure 17. Interface vs. time at $P_s = 10^{-6}$.

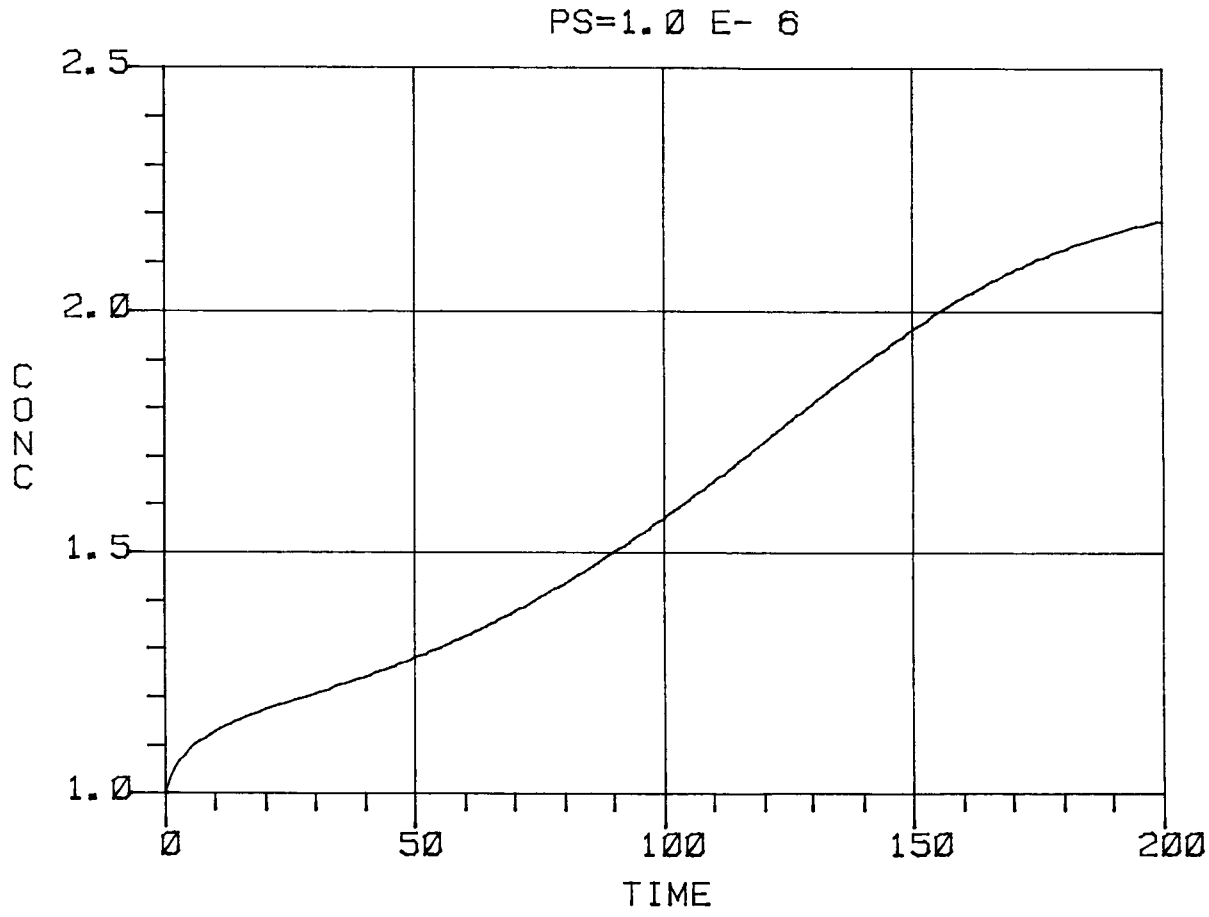

Figure 18. Concentration vs. time at $P_s = 10^{-6}$.

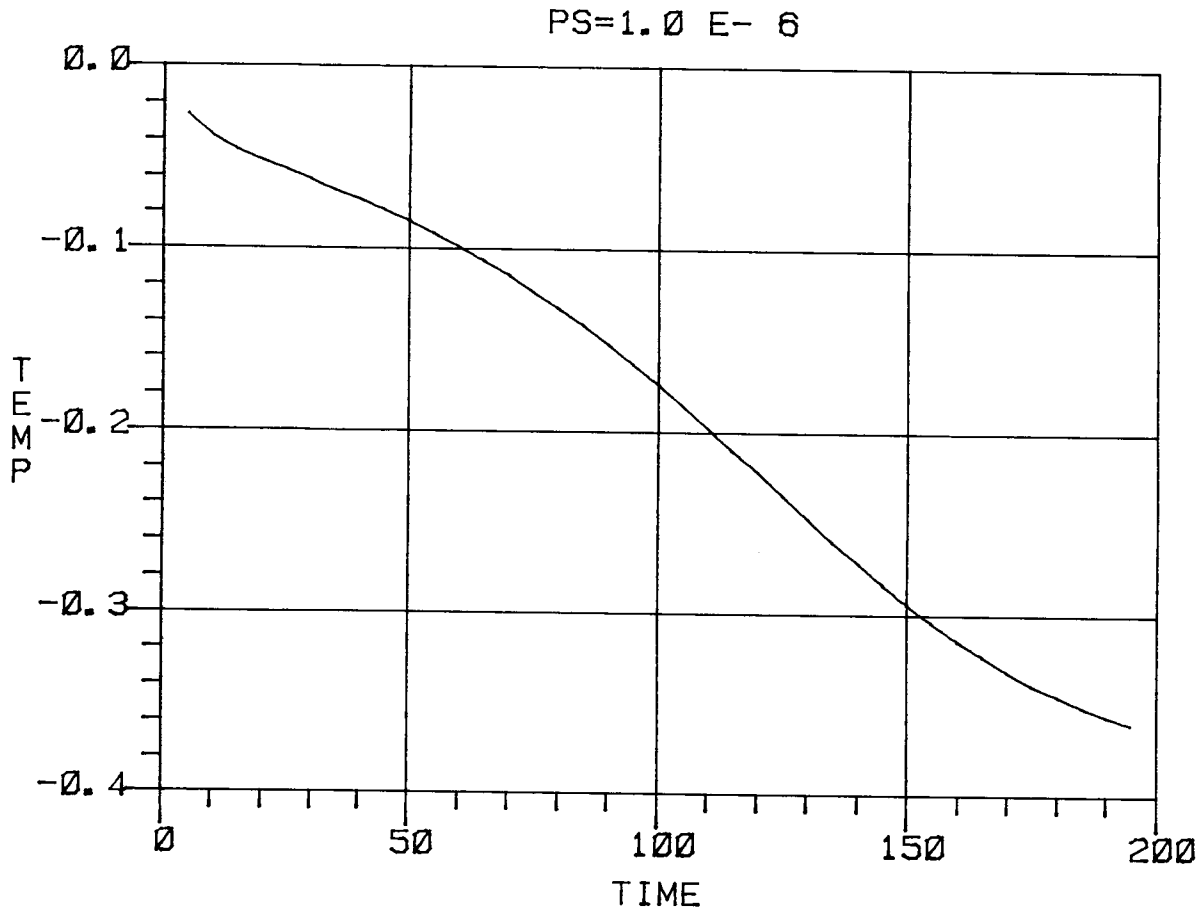

Figure 19. Temperature vs. time at $P_s = 10^{-6}$.

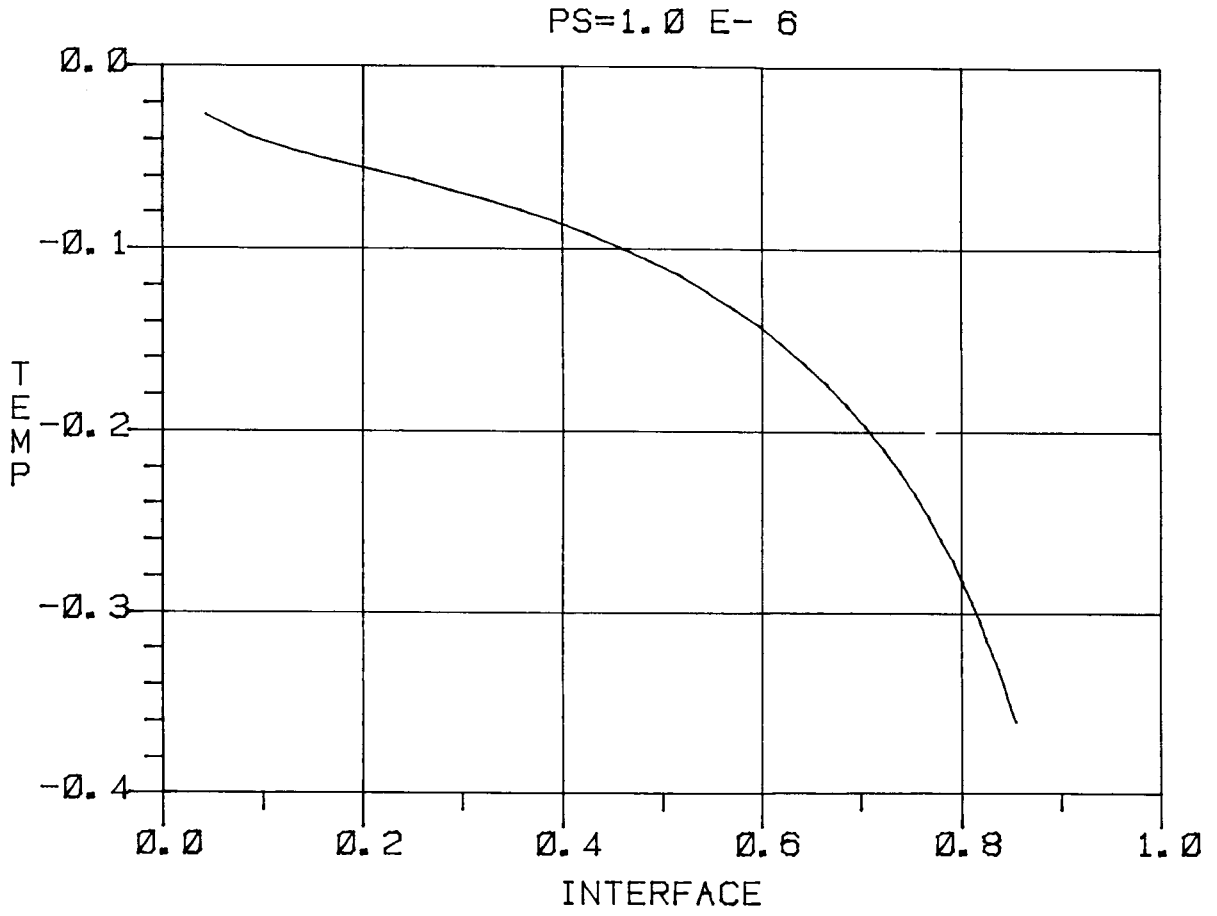

Figure 20. Temperature vs. interface at $P_s = 10^{-6}$.

certain value and then begins to increase. Allowances for this have not been made and since the concentration of the liquid will be ever increasing, the melting temperature will continually decrease, which can be seen in Figures 10, 12, 14, 16, 18 and 20. It is also interesting to note that the velocity of the interface is proportional to the Lewis number. The lower Lewis numbers cause slower solidification. Due to the slower diffusion rates, the interface concentration is higher and therefore the melting temperature is lower, requiring more time for the alloy to reach the melting temperature since the heat rates remain the same.

Figures 21-23 illustrate the effects of different densities in the solid and liquid phases. The interface moves at a slower rate when the density of the solid is greater than that of the liquid. The temperature and concentration with respect to time does not change significantly.

Figures 24-29 show the overall temperature and concentration distributions for the different Lewis numbers. The concentration distributions are represented by the solid lines and the temperature distributions by the dashed lines.

In Figure 30 we see the comparison of results obtained from the analytical method at $P_s = 10^{-6}$ (Figure 30-A) with intuitive results [13] deduced from the phase diagram to the limit of zero diffusivity in the solid (Figure 30-B).

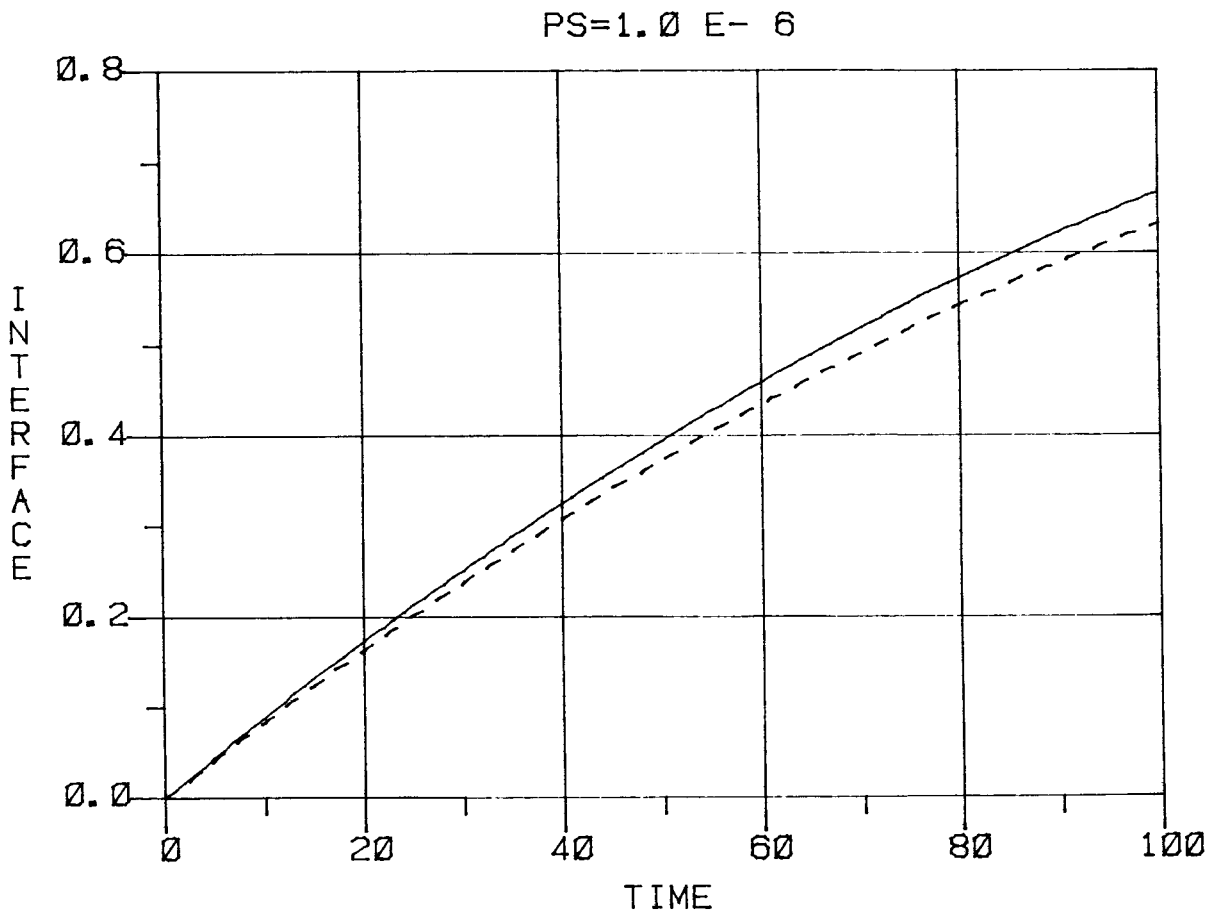

Figure 21. Comparison of interface vs. time for R = 1.00 and R = 1.06.

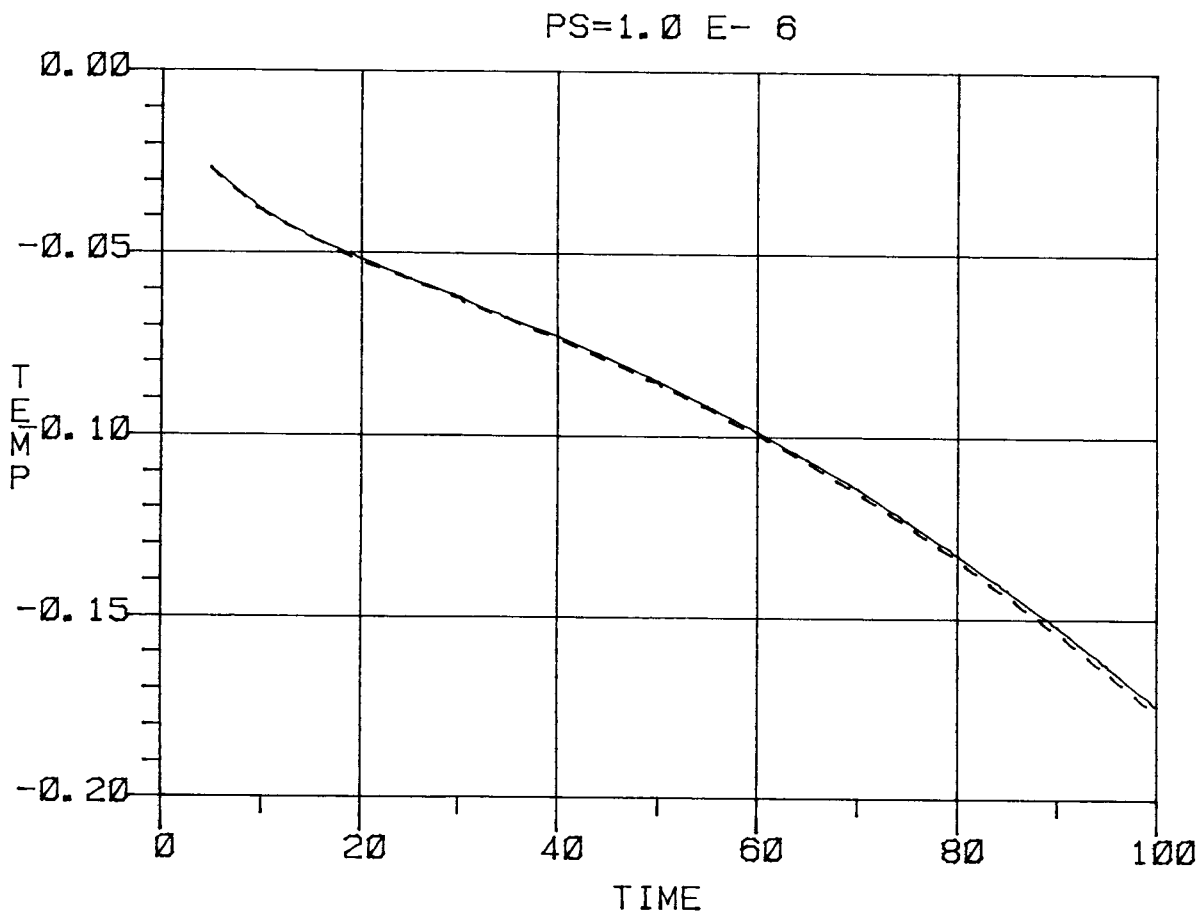

Figure 22. Comparison of temperature vs. time for R = 1.00 and R = 1.06.

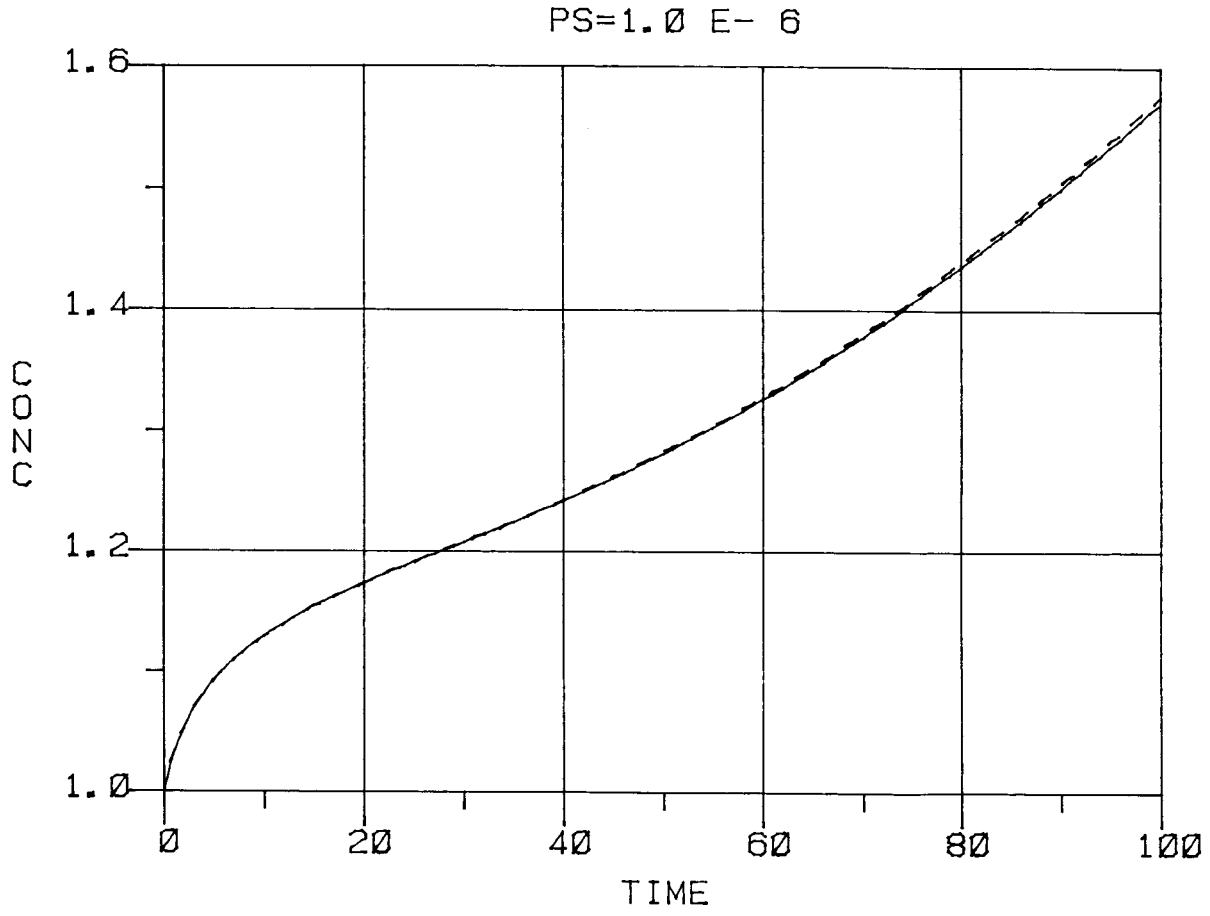

Figure 23. Comparison of concentration vs. time for R = 1.00 and R = 1.06.

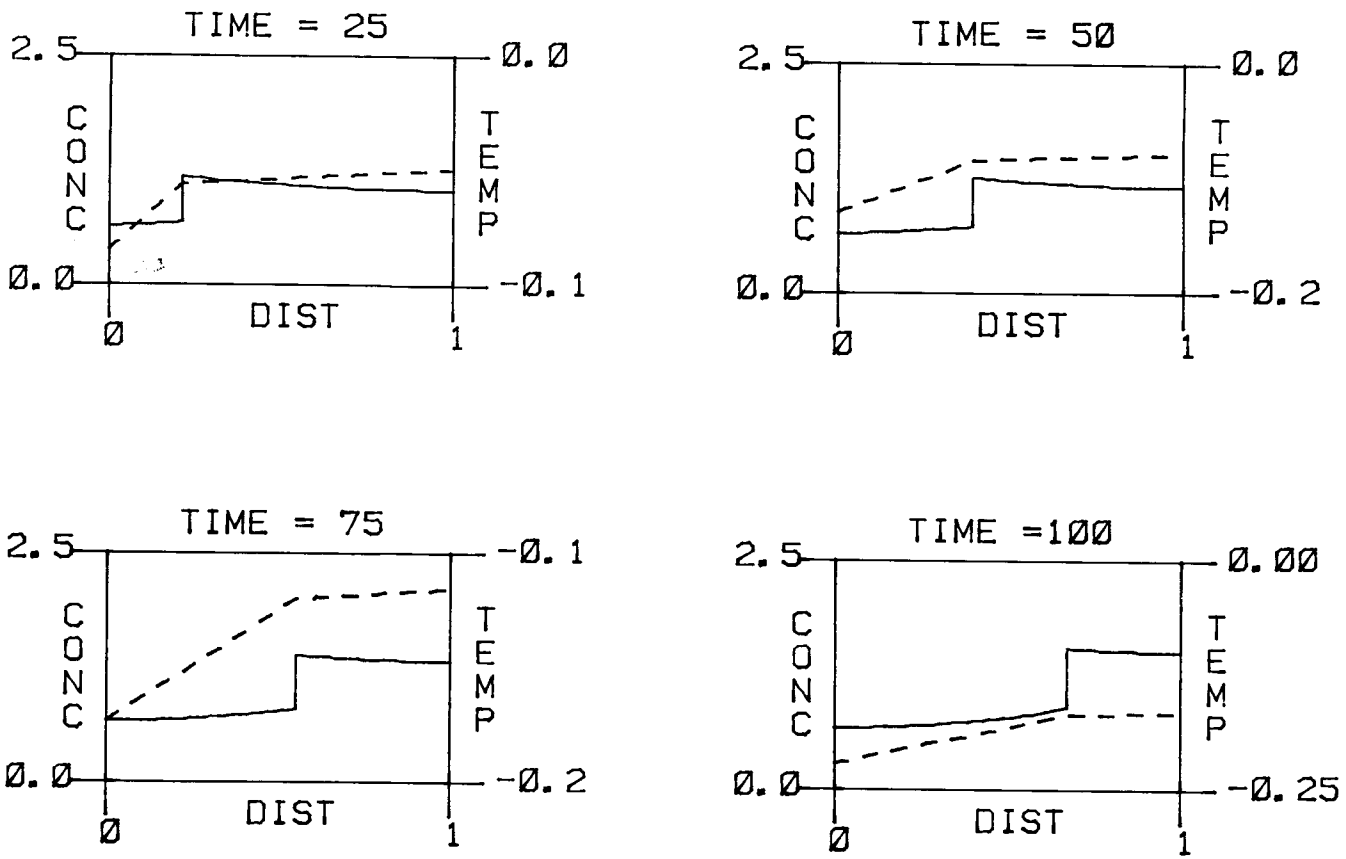

Figure 24. Temperature and concentration distributions for time = 25 - 100 with $P_s = 10^{-4}$.

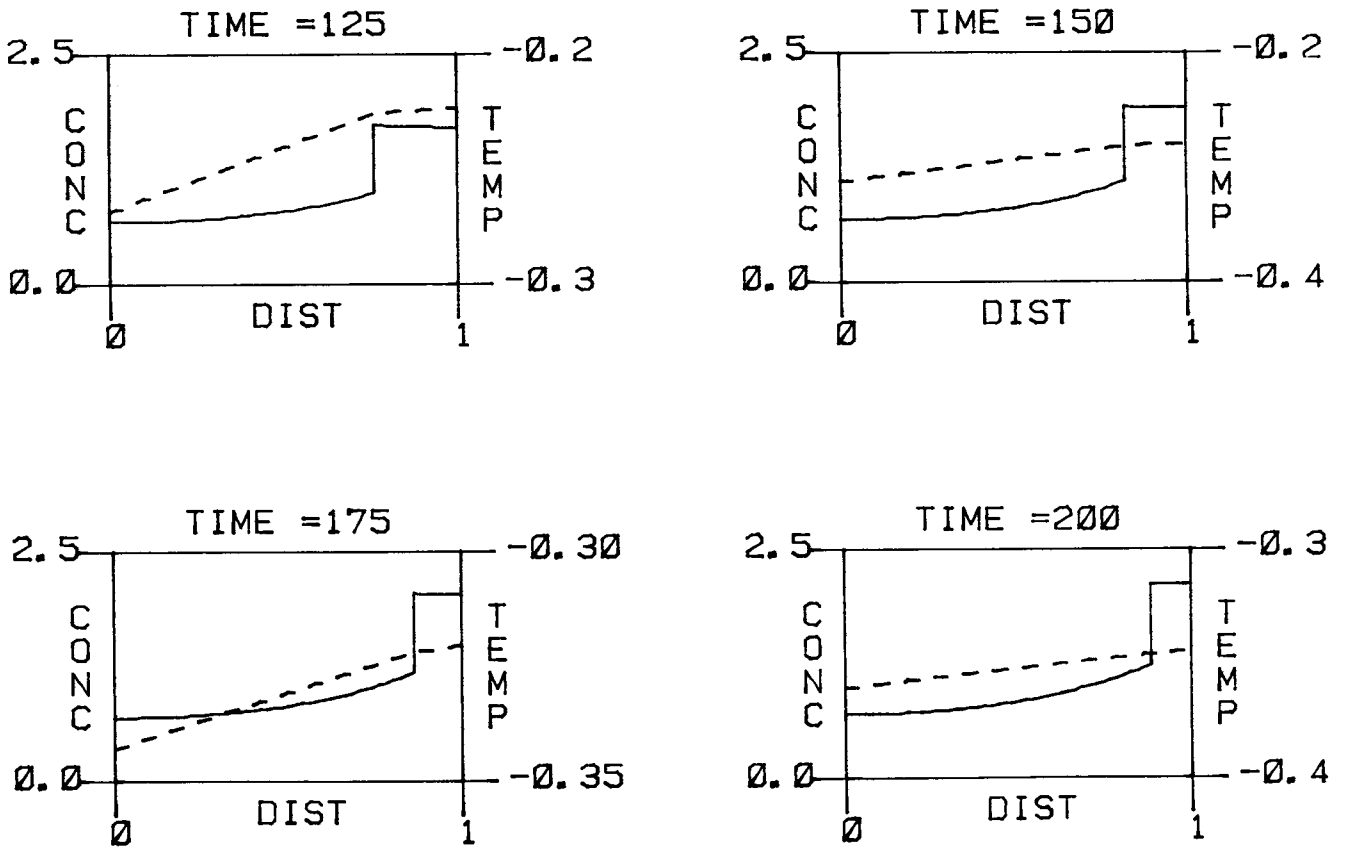

Figure 25. Temperature and concentration distributions for time = 125 - 200 with $P_s = 10^{-4}$.

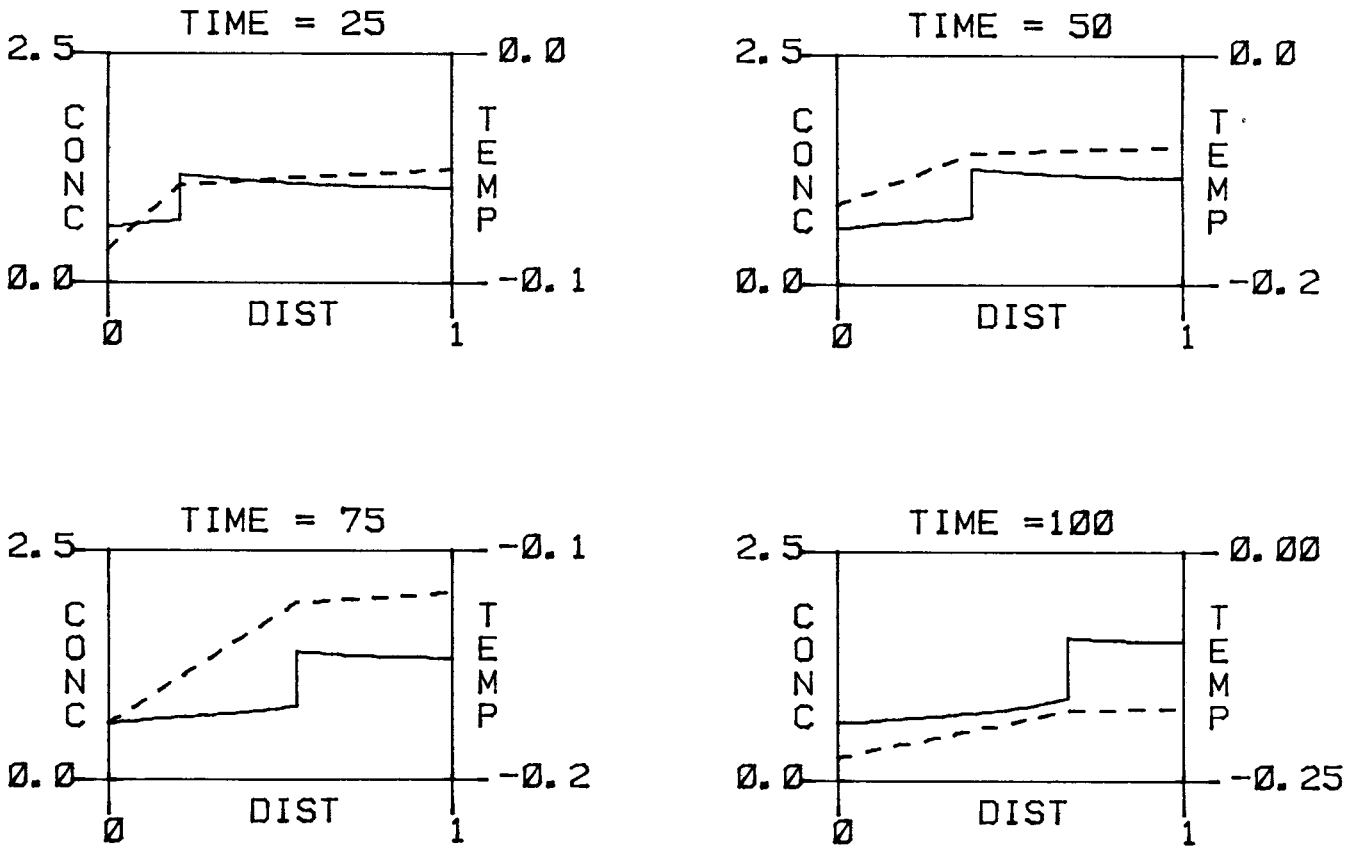

Figure 26. Temperature and concentration distributions for time = 25 - 100 with $P_s = 10^{-5}$.

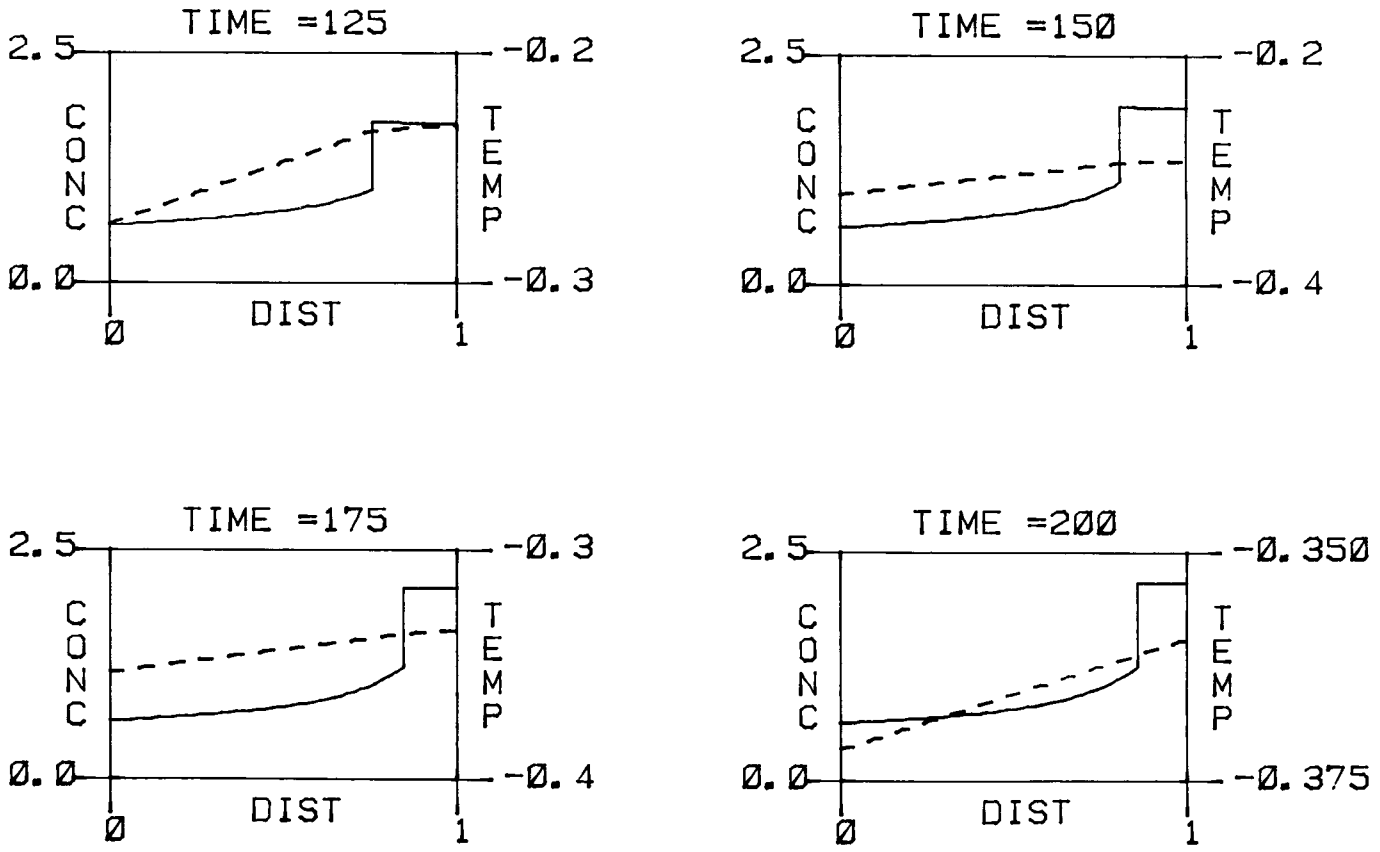

Figure 27. Temperature and concentration distributions for time = 125 - 200 with $P_s = 10^{-5}$.

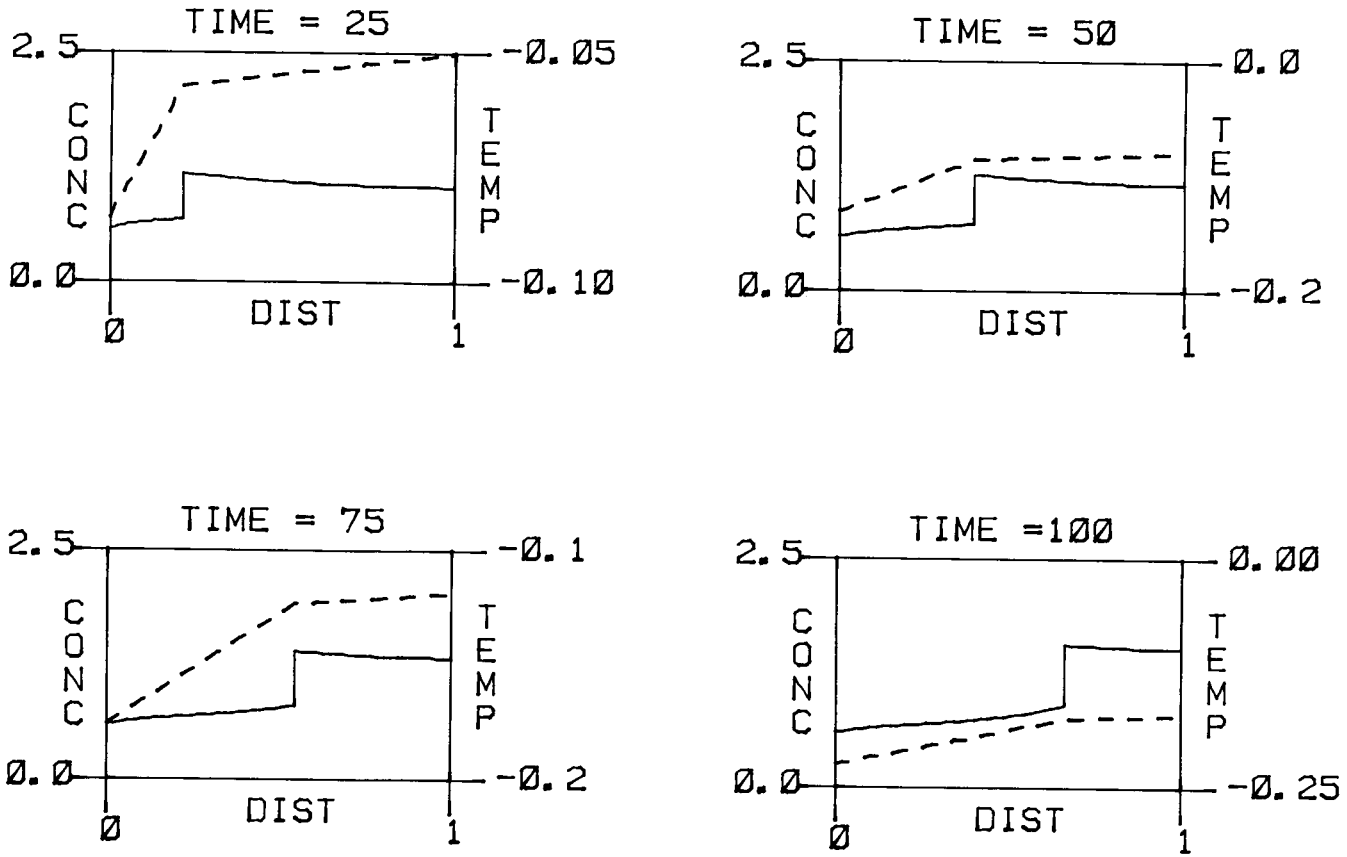

Figure 28. Temperature and concentration distributions for time = 25 - 100 with $P_s = 10^{-6}$.

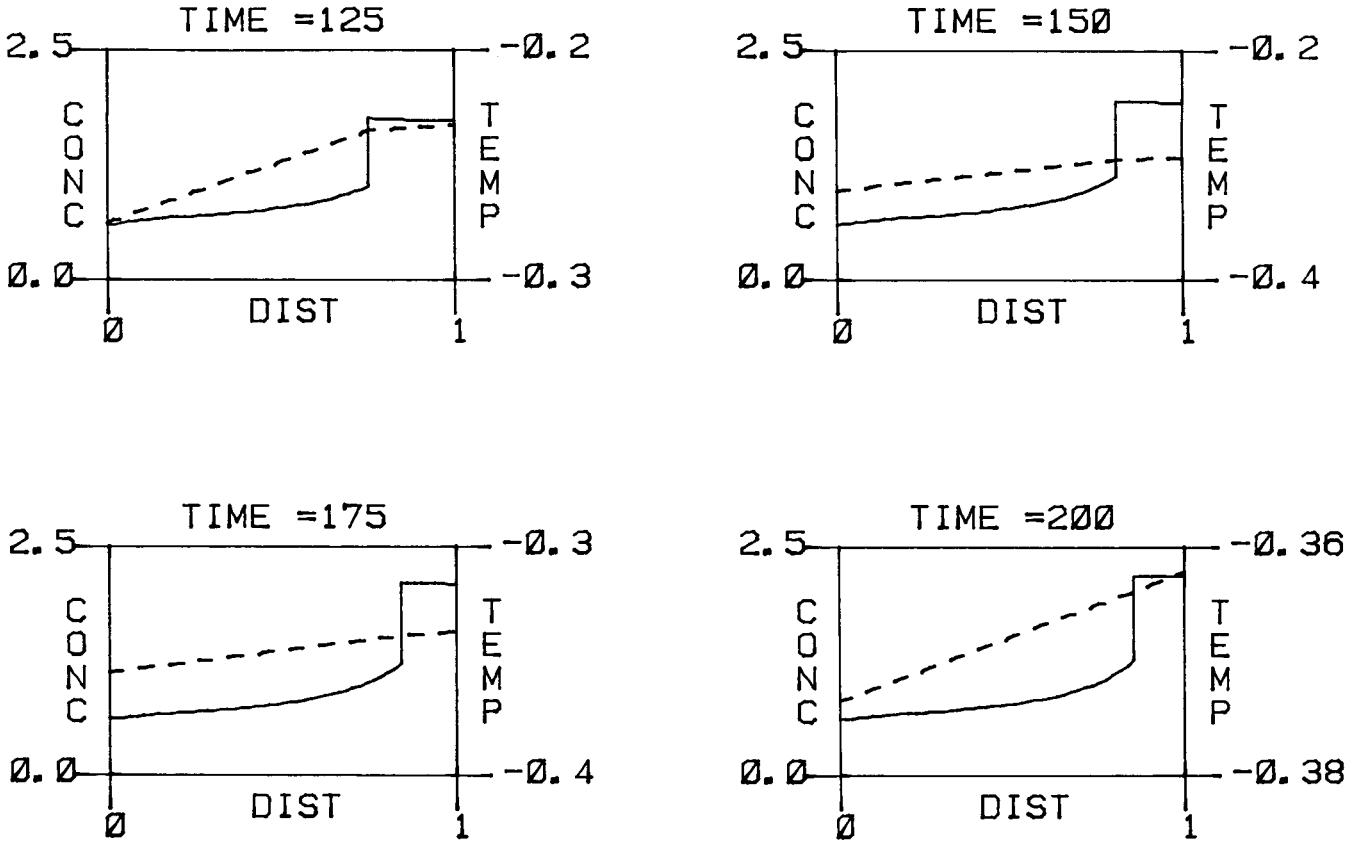

Figure 29. Temperature and concentration distributions for time = 125 - 200 with $P_s = 10^{-6}$.

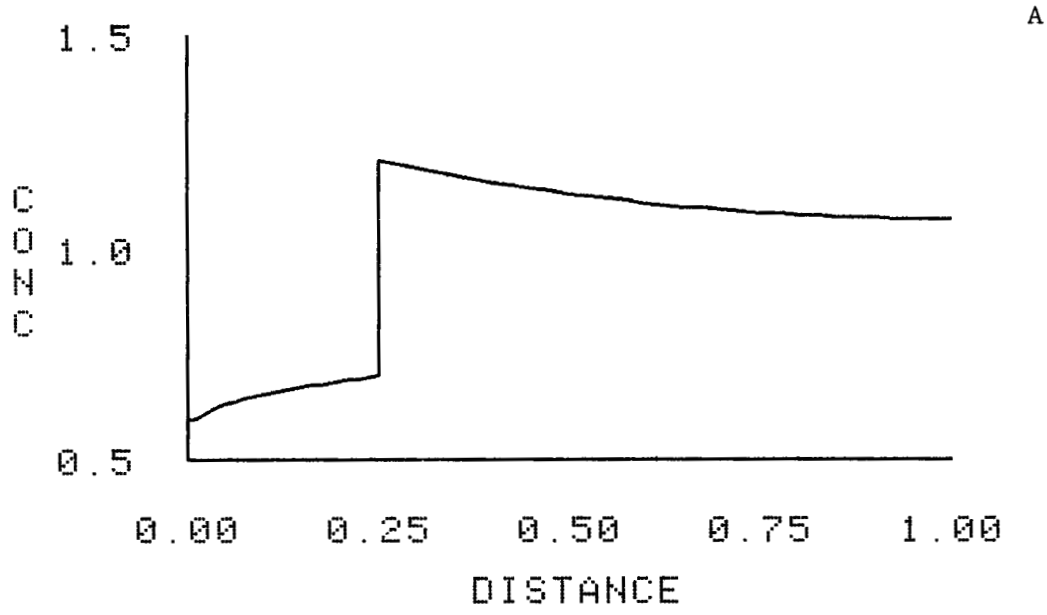

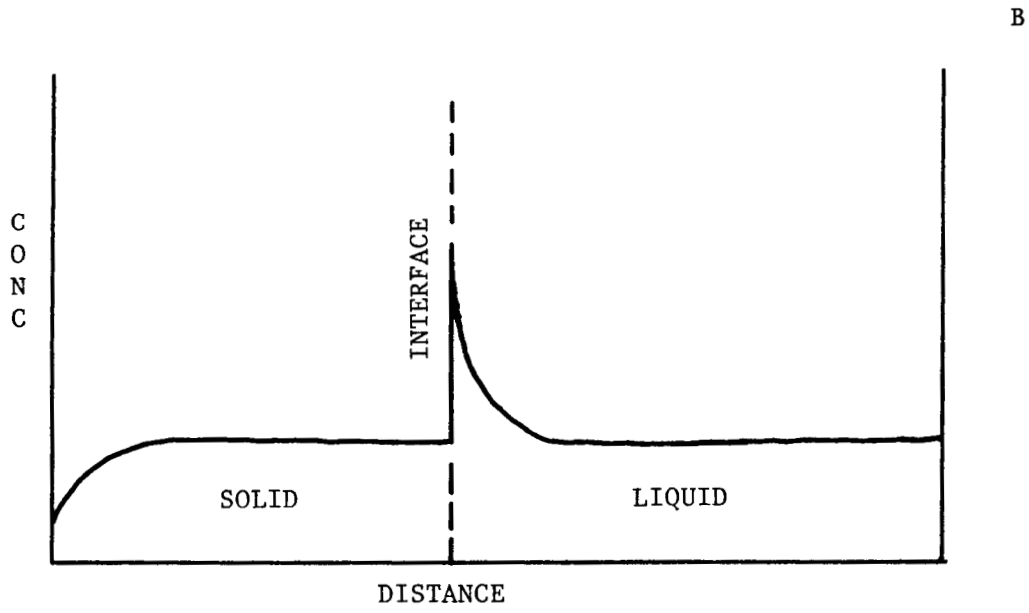

Figure 30. Comparison of analytical method at $P_s = 10^{-6}$ with intuitive results from reference [13].

LIST OF REFERENCES

1. American Society for Metals, Metals Handbook, Eighth Edition, Volume 8, Metals Park, Ohio, 1973.

2. Antar, Basil N. "Solidification of a Binary Mixture", In Research Reports--1981 NASA/ASEE Summer Faculty Fellowship Program, G. R. Karr, J. B. Dozier, M. I. Kent and B. F. Bartfield, Editors, NASA CR-161855, 1982.

3. Boley, Bruno A. "Time Dependent Solidification of Binary Mixtures". Int. J. Heat and Mass Transfer. Vol 21, No. 6, p. 821-824, 1978.

4. Burden, R. L., Faires, J. D. and Reynolds, A. C. Numerical Analysis. Boston: Prindle, Weber and Schmidt, 1981.

5. Carnahan, B. Applied Numerical Methods. New York: John Wiley and Sons, 1969.

6. Carslaw, H. S. and Jaeger, J. C. Conduction of Heat in Solids. London: Oxford University Press, 1959.

7. le Claire, A. D. "Diffusion of Metals in Metals", Progress in Metal Physics, Chalmers, B., Editor. London: Pergamon Press, 1961.

8. Coriell, S. R. and Cordes, M. R. and Boettinger, W. J. "Convective and Interfacial Instabilities During Unidirectional Solidification of a Binary Alloy". Journal of Crystal Growth. 49 (198) 1979.

9. Ince, E. L. Ordinary Differential Equations. New York: Dover, 1956.

10. Fehlberg, E. "Klassische Runge-Kutta-Formeln Funfter und Siebenter Ordnung Mit Schrittweiten-Kontrolle." Computing. 4, p. 93-106, 1969.

11. Meyer, G. H. "On a General Theory of Characteristics and the Method of Invariant Imbedding". SIAM J. Appl. Math. Vol. 16, No. 3, p. 488-509, May 1959.

12. _____. "A Numerical Method for the Two-Phase Stefan Problem". SIAM J. Numer. Anal., Vol. 8, No. 3, p. 555-568, Sept. 1971.

13. Naumann, R. J. and Herring, H. W. Materials Processing in Space: Early Experiments. NASA SP-443, 1980.

14. Ockendon, J. R. and Hodgkins, W. R. Moving Boundary Problems in Heat Flow and Diffusion. London: Oxford University Press, 1975.

15. Ozisik, M. N. Heat Conduction. New York: John Wiley and Sons, 1980.

16. Reid, W. T. Riccatti Differential Equations. New York: Academic Press, 1972.

17. Rubenstein, L. I. The Stefan Problem. Rhode Island: American Mathematical Society, 1971.

18. Tao, L. N. "On Solidification of a Binary Alloy". Q. J. Mech. Appl. Math. Vol. 33, pt. 2, p. 211-225, 1980.

1. REPORT NO.	2. GOVERNMENT ACCESSION NO.	3. RECIPIENT'S CATALOG NO.
NASA CR-3962		

4. TITLE AND SUBTITLE	5. REPORT DATE
An Exact Solution for the Solidification of a Liquid Slab of Binary Mixture	March 1986
	6. PERFORMING ORGANIZATION CODE
7. AUTHOR(S) B. N. Antar, F. G. Collins, and A. E. Aumalis	8. PERFORMING ORGANIZATION REPORT #
9. PERFORMING ORGANIZATION NAME AND ADDRESS The University of Tennessee Space Institute Tullahoma, Tennessee 37388	10. WORK UNIT NO. M-513
	11. CONTRACT OR GRANT NO. NAS8-34268
12. SPONSORING AGENCY NAME AND ADDRESS National Aeronautics and Space Administration Washington, DC 20546	13. TYPE OF REPORT & PERIOD COVERED Final Report Jan. 2, 1985 Contractor Report
	14. SPONSORING AGENCY CODE

15. SUPPLEMENTARY NOTES

Technical Monitor: C. F. Schafer
Prepared for Systems Dynamics Laboratory, Geo. C. Marshall Space Flight Center

16. ABSTRACT

The time dependent temperature and concentration profiles of a one dimensional finite slab of a binary liquid alloy is investigated during solidification. The governing equations are reduced to a set of coupled, nonlinear initial value problems using the method outlined by Meyer in ref [11,12]. Two methods will be used to solve these equations. The first method uses a Runge-Kutta-Fehlberg integrator to solve the equations numerically. The second method comprises of finding closed form solutions of the equations.

17. KEY WORDS	18. DISTRIBUTION STATEMENT
Correction Binary Mixture Solidification Fluid Mechanics Stefan Problem	Subject Category: 44 Unclassified-Unlimited

19. SECURITY CLASSIF. (of this report)	20. SECURITY CLASSIF. (of this page)	21. NO. OF PAGES	22. PRICE
Unclassified	Unclassified	76	A05

For sale by National Technical Information Service, Springfield, Virginia 22161

NASA-Langley, 198